Quantitative structural determination of active sites from in situ and operando XANES spectra: From standard ab initio simulations to chemometric and machine learning approaches

(Article begins on next page)

08 November 2024

Quantitative structural determination of active sites from *in situ* and *operando* XANES spectra: from standard *ab initio* simulations to chemometric and machine learning approaches

Alexander A. Guda,[1] Sergey A. Guda,[1] Kirill A. Lomachenko,[2] Mikhail A. Soldatov,[1] Ilia A. Pankin,[1,3] Alexander V. Soldatov,[1] Luca Braglia,[4] Aram L. Bugaev,[1] Andrea Martini,[1,3] Matteo Signorile,[3] Elena Groppo,[3] Alessandro Piovano,[3] Elisa Borfecchia,[5,6] and Carlo Lamberti[1,7,*]

[1] The Smart Materials Research Institute, Southern Federal University, Sladkova Street 178/24, 344090 Rostov-on-Don, Russia

[2] European Synchrotron Radiation Facility, 71 avenue des Martyrs, CS 40220, 38043 Grenoble Cedex 9, France

[3] Department of Chemistry, INSTM Reference Center and NIS Interdepartmental Center, University of Turin, via Giuria 7, I-10135 Turin, Italy

[4] CNR-Istituto Officina dei Materiali, Laboratorio TASC in Area Science Park, S.S. 14 km 163.5, Basovizza, 34149 Trieste, Italy

[5] Haldor Topsøe A/S, Haldor Topsøes All´e 1, Kgs. Lyngby, 2800 Denmark

[6] Center for Materials Science and Nanotechnology (SMN), Department of Chemistry, University of Oslo, 1033 Blindern, 0315 Oslo (Norway)

[7] Department of Physics, INSTM Reference Center and CrisDi Interdepartmental Center for crystallography, University of Turin, via Giuria 1, I-10135 Turin, Italy. E-mail: carlo.lamberti@unito.it

Highlights

- Different theoretical methods in the simulation of the XANES spectra are discussed

- An extended list of available codes for XANES spectra simulation is provided

- The potential of operando XANES in catalysis is described with relevant examples

- Chemometric methods in the treatment of operando XANES spectra is discussed

- Machine learning approaches are used to provide structural determination from XANES

Abstract

In the last decade the appearance of progressively more sophisticated codes, together with the increased computational capabilities, has made XANES a spectroscopic technique able to quantitatively confirm (or discard) a structural model, thus becoming a new fundamental diagnostic tool in catalysis, where the active species are often diluted metal centers supported on a matrix. After providing a brief historical introduction and the basic insights on the technique, in this review article, we provide a selection of four examples where *operando* XANES technique has been able to provide capital information on the structure of the active site: (i) Phillips catalyst for ethylene polymerization reactions; (ii) TS-1 catalyst for selective hydrogenation reactions; (iii) carbon supported Pd nanoparticles for hydrogenation reactions; (iv) Cu-CHA zeolite for NH_3-assisted selective reduction of NO_x and for partial oxidation of methane to methanol. The last example testifies how the multivariate curve resolution supported by the alternating least-squares algorithm applied to a high number of XANES spectra collected under *operando* conditions allows to quantitatively determine different species in mutual transformation. This approach is particularly powerful in the analysis of experiments where a large number of spectra has been collected, typical of time- or space-resolved experiments. Finally, machine learning approaches (both indirect and direct) have been applied to determine, from the XANES spectra, the structure of CO, CO_2 and NO adsorbed on Ni^{2+} sites of activated CPO-27-Ni metal-organic framework.

1. Introduction

Technically speaking, X-ray absorption spectroscopy is divided into two parts, depending whether we are referring to the region near the adsorption edge (X-ray absorption near-edge structure, or XANES) or at higher energy with respect of the edge (extended X-ray absorption spectroscopy, or EXAFS) [1]. Although experimentally measured in the same data collection, XANES and EXAFS differ in the information that they can provide, and in the way the data will be handled.

On an historically point of view, the fine structure appearing in the X-ray absorption spectra in the some hundreds of eV range after the K (L) edge of the first (second) row transition element was known since one century [2-16]. Notwithstanding all these experiments, and all those that followed after the second world war, for a long time there was no unified theory for the interpretation of such features [17] and the technique has been unable to provide quantitative information on the local structure of the absorbing atom in the investigated samples. This impasse ended in 1971, when Sayers, Stern, and Lytle showed that the Fourier transform of the background-subtracted oscillations gives, in *R*-space, a pattern close to the function of radial distribution of atomic density [18]. This study represented the milestone for EXAFS spectroscopy that was further implemented later in more formal derivations (e.g. based on based on Green's function and generalization to muffin-tin scattering potentials, [19-23] or on the decomposition of the cross-section in the EXAFS region into irreducible n-body signals [24-26]). Starting from the 1970s, the increased availability of several and progressively more brilliant and broadband synchrotron radiation sources and the successive development and the distribution of different codes for the data analysis made EXAFS a diffuse and reliable structural characterization technique exploited by a large community worldwide, and being nowadays reported in more than 2000 scientific papers per year [27].

The historical evolution of XANES spectroscopy (which acronym was first introduced by Bianconi in 1980 [28]) has been quite different from the EXAFS one. In 1960, Van Nordsthand[29]

reported a systematic study on the XANES spectra of many transition metal compounds and classified their XANES spectra according to the atomic structure and valence of the metal element in the compound, also noting the chemical shift with valence. This fingerprint classification was used to identify the structural/valence form of elements in catalysts, which are usually highly dispersed on a support, so that their X-ray diffraction patterns does not produce Bragg peaks. Summarizing, already a decade before the paper that made EXAFS a useful structural characterization technique [18], XANES spectroscopy was already able to provide important insights. However, for several decades, the XANES spectra were used mainly in a qualitative way, measuring edge, shifts considering the presence/absence of certain fingerprint features and comparing the data with the spectra of model compounds [30-32]. In the XANES history a milestone was the appearance of the first code able to compute a theoretical spectrum starting from an hypothesized local structure: the CONTINUUM code by Natoli and co-workers [33, 34]. Successively, the appearance of progressively more sophisticated codes, together with the increased computational capabilities, has made XANES a spectroscopy able to quantitatively confirm, or discard a structural model for the environment of the X-ray absorbing atom [35-43], forming thus a new fundamental diagnostic tool in condensed matter physics and chemistry [44-48].

Moreover, the quantitative structural determination by simulation of XANES spectra from density functional theory (DFT) optimized structures is the only X-ray based available approach in case where the catalytic active site is highly diluted, a scenario that is quite common in catalysis. In such cases, the contribution of the diluted species to the X-ray scattering process is negligible and high-quality EXAFS spectra cannot be obtained in the high-k region, preventing the possibility to perform a detailed structural investigation by EXAFS.

In this manuscript, we summarize some relevant cases from the recent literature (2015-2018) and we report unpublished examples where an advanced analysis of the XANES data allowed to obtain unprecedented insights on the local structure of metal centers in relevant catalysts.

2. Methods
2.1. Theory of XANES

X-ray absorption spectroscopy in general, and XANES in particular, is a unique tool which can be applied *in situ* and under *operando* conditions to extract the local atomic and electronic structure of the catalytically active centers [35, 36, 41, 47, 49-86]. Fig. 1a shows the possible signal collection schemes adopted in a XAS experiment. The incoming polychromatic synchrotron radiation from bending a magnet, a wiggler or an undulator propagates through the primary monochromator and reaches the sample. Ionization chambers are used to measure incident and transmitted intensities, whereas silicon drift detectors are suited to record fluorescence, thus avoiding the spectroscopically irrelevant elastic scattering contribution. A second monochromator can be used to select given energy of the fluorescence, thus limiting the spectral broadening due to the core-hole lifetime [87]. The later scheme is referred as high energy resolved fluorescence detection (HERFD) mode.[80, 88, 89]
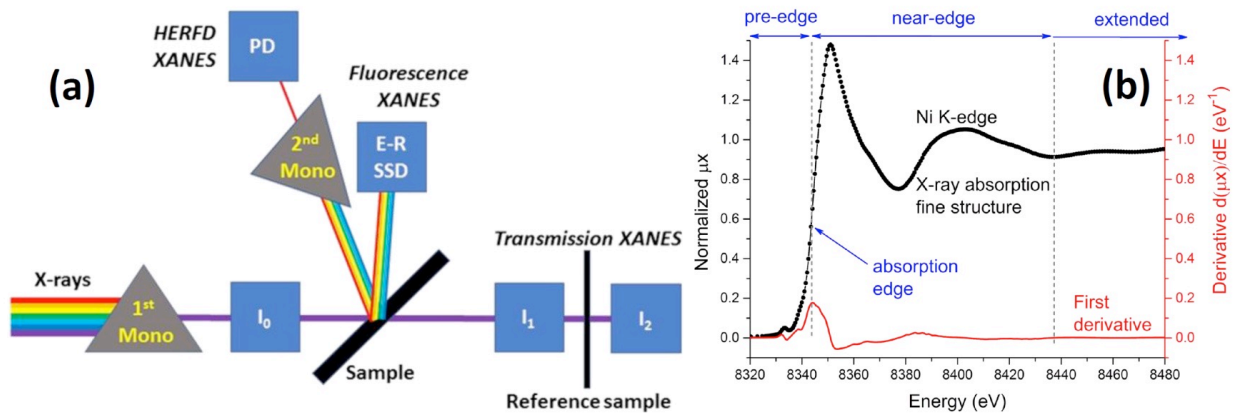
Fig. 1. Part (a): possible signal collection schemes adopted in a XAS experiment. In the optic hutch, the primary monochromator (eventually supported by mirror(s) for beam focusing and harmonics rejection) selects the incident beam energy, abscissa axis in part (b). In the experimental hutch, transmission XAS requires the use of two ionization chambers I_0 and I_1 to measure the incident and transmitted fluxes, respectively. The XAS spectrum is obtained as $\mu x = \ln(I_0/I_1)$. In time resolved *operando* experiments, a third ionization chamber (I_2) is recommended to guarantee a perfect energy calibration of each spectrum via the simultaneous measure of the XAS spectrum of a reference sample $\mu x_{Ref} = \ln(I_1/I_2)$. Alternatively, the XAS spectrum can be detected measuring I_0 and the fluorescence decay I_F: $\mu x = I_F/I_0$. The latter is usually measured by selecting the Kα and Kβ lines of the excited element from the Kα and Kβ lines of all the other elements present in the sample (and from the elastically scattered photons) through an energy-resolved, solid-state detector (E-R SSD, ΔE = 100-300 eV). Alternatively, fluorescence photons can be discriminated with improved energy resolution (ΔE = 0.5-5 eV) by analyzing them with a second monochromator, thus delectating the signal with a photodiode (PD); this specific configuration is referred as HERFD XAS. Part (b): a typical XANES spectrum (black curve) and its first derivative with respect to energy (red curve), highlighting the pre-edge, near-edge and extended spectral regions. The spectrum refers to the Ni K-edge of dehydrated CPO-27-Ni MOF in interaction with NO (see Section 3.5 for discussion on this example).

Fig. 1b shows the common notation describing X-ray absorption spectra. Extended X-ray absorption fine structure, when properly measured, can provide information about coordination numbers and interatomic distances [90]. However, single scattering events dominating the EXAFS signal do not contain information about bending angles, as necessary to elucidate the problem of adsorbate molecules on the catalytically active centers. Thereby, XANES features should be analyzed instead. Theoretical methods and computational software developed over the last two decades can perform accurate theoretical XANES simulations, based on the theory on interaction of electromagnetic radiation with the matter. The total energy of a particle in an electromagnetic field is given by a Hamiltonian (H) obtained by adding to the ground state Hamiltonian (H_0) a time-dependent potential ($V(t)$):

$$H = H_0 + V(t) \qquad (1)$$

The interaction of an electron in a molecule/solid with an incident electromagnetic X-ray radiation is described by the perturbation theory. A simplified (but practically important) formalism to describe the one-electron dipole absorption cross section for the transition from 1s core level into continuum final states is Fermi's golden rule [91-94], first formalized by Dirac [95]:

$$\sigma(h\nu) = 4\pi^2 \alpha h\nu \left| \langle \psi_i | \boldsymbol{\varepsilon} \cdot \boldsymbol{r} | \psi_f \rangle \right|^2 \rho_{occ}(E_i)\rho_{unocc}(E_f)\delta(E_f - E_i - h\nu) , \qquad (2)$$

4

where $\boldsymbol{\varepsilon} \cdot \boldsymbol{r}$ is the dipole operator, $h\nu$ is the energy of the absorbed photon, h is the Plank constant ($h = 6.62607 \times 10^{-34}$ m^2 kg s^{-1}), $\alpha = 1/137$ is the fine structure constant, $\rho_{occ}(E_i)$ and $\rho_{unocc}(E_f)$ are respectively the occupied (initial) and unoccupied (final) density of states (DOS), and where the delta of Dirac function guarantees the energy conservation by imposing the $E_f = E_i + h\nu$ condition. The main difficulty in calculating the cross section for real system arises from the final state wavefunction ψ_f in molecules or electron DOS ρ for solids. In a first step of the wavefunction calculation, the electron potential, including the electron-nuclei and the electron-electron interactions, should be computed. DFT is conceived to treat ground-state electron-electron interactions [96] and is consequently inadequate to simulate spectra involving electron transitions, since these require the description of both ground and excited states. Consequently, spectra calculations involving electronic transitions (UV-Vis (ultraviolet-visible), luminescence, UPS (ultraviolet photoelectron spectroscopy), XPS (X-ray photoelectron spectroscopy), XANES etc.) are performed in the frame of time-dependent DFT (TDDFT) [97-104]

The proper description of the pre-edge region of XANES spectra, $L_{2,3}$ edges of 3d metals and excitonic effects requires the many body corrections which can be treated by: (i) using the multiplet approach [105, 106]; (ii) solving the Bethe-Salpeter equation (BSE) [107-111]; (iii) applying post Hartree Fock (HF) methods [112, 113]; (iv) by using the dynamic mean field theory (DMFT) [114]; or by expanding off the many-electron system self-energy in a series of products of Green functions and the screened Coulomb interaction (GW) [115, 116]. BSE, post-HF and DMFT approaches are beyond the scope of present paper and are not further discussed in the following.

Transition from the core state to the final state can be approximated by the final state rule (the wavefunction ψ_f is calculated in the presence of a static core hole), or by using TDDFT [117]. Table 1 summarizes the list of approaches and available software for this task. The corresponding one-electron Schrödinger equation can be solved by using alternatively: (i) the Green function approach [22, 118]; (ii) the finite difference method [37, 38, 48, 119, 120]; (iii) or by expanding the unknown wavefunction into a series of basis set functions [121, 122]. For the last case, plane wave basis (widely used in solid state physics), cannot be straightforwardly applied because the required pseudopotential approximation cannot account for the presence of a core hole. Nowadays this problem is solved in the program package Quantum Espresso [122-126] and its extension Xspectra [127, 128], which allow efficient modeling of the excitonic effects in compounds with almost empty d-shell. Unfortunately, its application to the middle-row 3d elements still requires further investigations. Application of this approach for the high-energy resolved x-ray absorption spectra is shown elsewhere [129].

Several DFT-based codes with localized orbitals in a basis set, such as ADF [130] and ORCA [131, 132], are able to directly compute the pre-edge region within the TDDFT approximation. TDDFT can provide reasonable values for XANES cross-section up to 40 eV above the absorption edge [133, 134], and other techniques are being developed to access higher-lying electronic core-excited states, e.g. an algebraic-diagrammatic construction scheme [135]. Recently we have shown that for the near edge structure of metallorganic complexes simplified to the frozen orbitals

TDDFT approximation provides already good agreement between experimental and calculated spectra [136, 137].

Table 1. Classification of the methods to calculate XANES spectra and available software for calculations. The references for the software are following: FEFF 9.0 [45, 118, 138], CONTINUUM [33, 34], FDMNES [37, 38, 48, 119, 120], XKDQ [139, 140], SPRKKR [141, 142], MXAN [143-148], ADF [130], ORCA [131, 132], Gaussian [149], Quantum Espresso [122-126], Wien2k [150-156], PARATEC [127], Quanty [157], XTLS [158], CTM4XAS [159], OCEAN [110, 111], MOLCAS [160-163] EXC!TiNG [109, 116, 164], ONETEP [165].

XANES simulations							
DFT, TDDFT			**Many-body**				
Green Function	Finite difference	Basis set	Atomic multiplets	GW	BSE	post HF	DMFT
FEFF	FDMNES	ADF	QUANTY	EXCITING	OCEAN	MOLCAS	ONETEP
CONTI-NUUM		ORCA	XTLS	FEFF	EXCITING	ORCA	Quanty
FDMNES		Gaussian	CTM4XAS				
SPRKKR		Wien2k					
MXAN		Quantum Espresso					
XKDQ		PARATEC					

The Finite Difference Method (FDM) is attractive for calculations of the photoelectron wave function up to 100-200 eV above the absorption edge. It avoids in a simple way the muffin tin approximation [166] used in most of the quoted softwares, for example in those based on the multiple scattering theory (MST). In the latter approximation, the potential is assumed to be spherical inside the touching (or overlapping) atomic spheres and constant between them. However, in some cases the MST scheme might be not fully applicable, especially when the studied compound is sparse or with strong covalent bonds.

Taking as example the CPO-27-Ni MOF upon interaction with carbon monoxide (Fig. 2a and section 3.5), we show in Fig. 2b how the space around a Ni^{2+} ··CO molecular complex is divided to avoid muffin-tin approximation in an efficient way [119]. The potential is defined to be constant outside a sphere of chosen radius centered on Ni atom (i.e. the region with no atoms outside the blue circle) and spherically symmetric inside small spheres centered at atomic positions (diameter around 0.5-0.7 Å, marked by red and black colors). No restrictions on the potential are set for the intermediate region where interpoint distance equals to 0.2 Å. The wave function in the intermediate region is then obtained by solving the Schrödinger equation via the finite difference

method. In the regions with constant or spherically symmetric potential the wave function is represented by Neumann and Bessel (or Hankel) functions and as a multipole expansion around the center as shown in the figure [119].

The FDMNES (finite difference method near edge structure) project [48, 119, 120] aims to provide a user-friendly tool for the accurate XANES[37, 38] and resonant X-ray diffraction (RXD) [167] simulations. Recently we have implemented sparse solvers to significantly accelerate the code.[37] We have shown how spin-polarized electron density can be imported from quantum chemistry calculations for the finite difference calculations and used subsequently to predict spectra for the intermediate states of the 3d metal complexes. Both these effects make accurate FDMNES method a unique instrument for the structural refinement using machine learning (ML) strategies, as it will be described in Section 3.5.
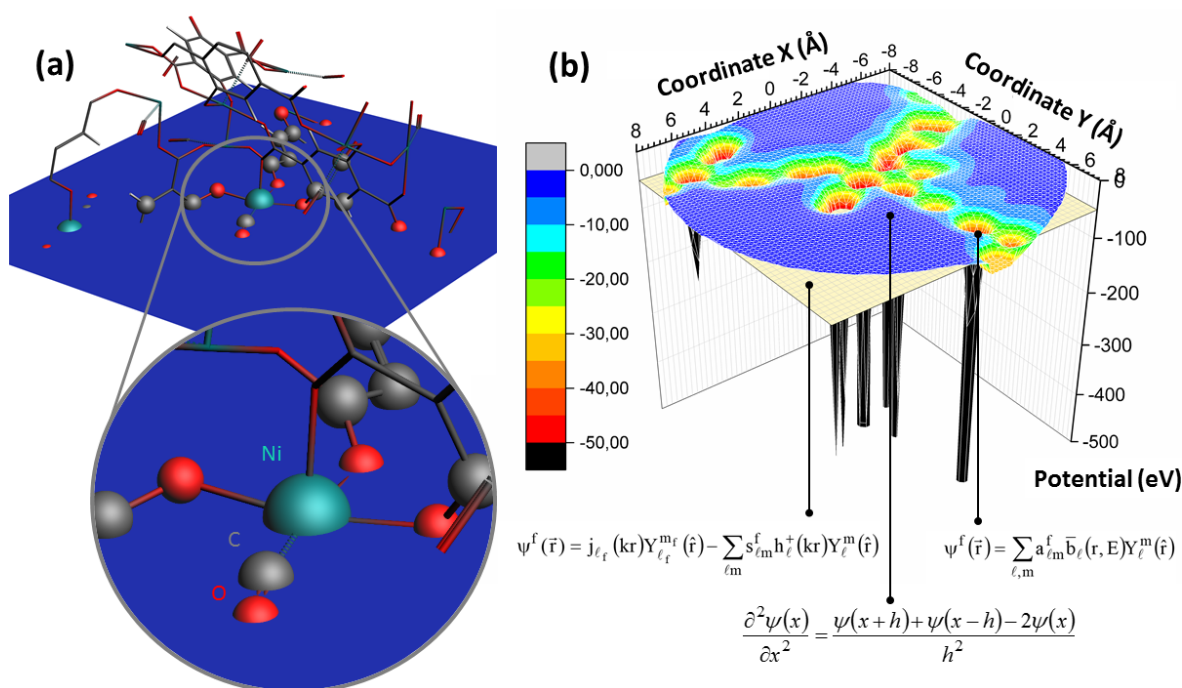

Fig. 2. Part (a): VASP optimized structure of activated CPO-27-Ni MOF with a CO molecule adsorbed on the coordination vacancy of Ni^{2+} [168]. Ni, C and O atoms are represented by cyan, gray and red balls/sticks, respectively. Evidenced in blue is the plane passing by the Ni, C and O atoms of the $Ni^{2+}\cdots CO$ adduct. Part (b): Total potential for the electron calculated on the two-dimensional grid of points taken on the blue plane defined in part (a) by using FDMNES software. Color code of the bars represents the values of the potential.

2.2. The multivariate curve resolution (MCR) - alternating least-squares algorithm (ALS) methods in the analysis of operando XANES spectra

Multivariate curve resolution (MCR) methods allow to model an experimental dataset as the product of a spectral matrix **S**, composed by a minimal-uncorrelated set of pure spectra, for their signal-related concentration profiles, ordered in a matrix **C** [169].This kind of data factorization can be realized through an iterative alternating least-squares algorithm (ALS) called MCR-ALS, developed by Tauler and co-workers [170-172]. It is remarkable that this multivariate technique seems to be able to isolate the data-source of variation without any assumption about the individual

chemical/physical species contributing to the global signal response. As the first step, the algorithm requires to determine the number of pure species (i.e. pure spectra) in the multicomponent data mixture. This information can be known beforehand or determined by using principal component analysis (PCA) and some statistical estimators such us: the analysis of the components variance (scree plot), the Malinowsky IND-factor and F-Test [173-175]. The MCR-ALS routine must be initialized through the estimation of pure spectra or concentration profiles. For this purpose, references spectra or specific techniques apt to generate them, e.g. SIMPLISMA and the Evolving Factor Analysis (EFA), are used [176, 177]. Once that the initial estimates have been identified, the ALS procedure can take place. For each iterative cycle, matrices $\mathbf{S}$ and $\mathbf{C}$ are calculated and updated until the convergence is achieved. Along this process, different constraints can be applied to the recovered spectra and concentration profiles such as: non-negativity, unimodality and the mass balance condition [169]. It is worth noticing that the choice of an appropriate set of constraints is helpful in order to provide a chemical/physical meaning to the spectra and concentration profiles and to reduce the rotational ambiguities that affect the MCR methods [178]. The process' convergence is usually controlled through a figure of merit related to the model fit called lack of fit (%LOF). When the difference of the model fit between consecutive iteration does not improve significantly (*i.e.* a difference lower than 0.1% in the %LOF related to two consecutive iterations), the routine terminates providing the optimized forms of $\mathbf{S}$ and $\mathbf{C}$ as output [169, 172].

In the field of XAS, the use of MCR-ALS algorithm is continuously expanding on different topics: ion batteries [179], quantum dots [180], solid-state chemistry [181], and heterogeneous catalysis [182-188]. The MCR method has also been applied for analyzing Fe^{3+}/Fe_{total} in oxidation state of iron in amphiboles from micro-XANES data [189], an analytical problem that is very relevant in hearth science [190, 191].

From the listed references, it is evident that the MCR-ALS method applied to *operando* XANES spectra represents a powerful analytical approach to determine the quantitative speciation of chemical species in mutual transformation. This is crucial in time resolved experiments, typical of the *operando* investigation of a working catalyst, but can be relevant also in the analysis of space resolved experiments exploiting the micro and nano-focus beamline operative at third and fourth generation synchrotron radiation facilities [192]. A detailed example of the potentialities of this approach is reported in Section 3.4.

2.3. Machine learning

Machine learning (ML) represents a group of data analysis methods which are closely related to computational statistics and is used to solve problems of classification, regression, clustering, distribution analysis, dimensionality reduction, etc. [193]. ML exploits computer algorithms to predict the value of the unknown function on the basis of a training sample without being explicitly programmed for a given task [193]. This property makes ML a tool of increasing popularity in material science. As an example, once trained on a big set of DFT simulations, ML models can be applied to predict properties of new structures without performing the time-consuming simulations explicitly for them [194, 195]. ML techniques were already applied to a variety of problems of interatomic interactions: these include the correction of DFT potentials for the simulation of water polymorphs structures [196], the investigation of oxygen interactions at Pd surface [197], the bypass of Kohn-Sham equations for molecular dynamics [198, 199] and the prediction of DFT Hamiltonians with Kernel Ridge Regression [200]. Accurate and fast prediction of interatomic

potential energy can be further exploited for the discovery of new chemical compounds, as was shown in [201] for spin-crossover complexes.

ML can be applied to the quantitative analysis of spectroscopic data too. Zheng et al. have applied ML algorithms to XANES data to predict the correct oxidation state and coordination environment of a wide set of compounds, by accounting on a large dataset of spectra calculated within the muffin-tin approximation [202]. In this work an Ensemble-Learned Spectra Identification (ELSIE) algorithm was exploited: it combines 33 weak "learners" comprising a set of preprocessing steps and a similarity metric, and can achieve up to 84.2% accuracy in identifying the correct oxidation state and coordination environment. Timoshenko et al. used supervised ML (SML) to predict three-dimensional structure of metallic nanoparticles [203]. SML was used to unravel the hidden relationship between the XANES features and Pt nanoparticle (NP) geometry in Pt supported catalysts. To train the SML method, the authors relied on *ab initio* XANES simulations (see Section 2.1.). Their approach allowed to solve the structure of a metal catalyst from its experimental XANES, as demonstrated by reconstructing the average size, shape, and morphology of well-defined platinum nanoparticles. This method was applicable to the determination of the nanoparticle structure in *operando* studies and can be generalized to other nanoscale systems. Finally, the method of quantum clustering developed by Vainstein and Horn [204, 205] can be mentioned: though it is regarded as a machine learning approach for spectral analysis, it was not used widely afterwards.

In the present work we use different ML methods based on ensembles of random trees and ridge regression. In Section 3.5 we apply these methods to predict directly the geometry of active Ni center in CPO-27-Ni MOF upon gas adsorption. Results of ML studies are compared to the XANES fitting procedure by minimizing the integral square difference between theoretical and experimental spectra.

3. Selected examples

3.1. Molecular insights into Cr^{6+}/SiO_2 catalyst during C_2H_4 polymerization

The present predictions of the global demand for polyethylene (PE) resins for 2018 is of almost 10^8 tons, corresponding to a commercial value of more than $1.5 \ 10^{11}$ US \$, with an expected rise of 4.0% per year in the close future [206]. In this market, the Phillips catalyst (Cr/SiO_2) [207, 208] covers almost 40% of the high density PE world demand [209, 210]. Notwithstanding the industrial relevance of this catalyst, and the fact that it was patented almost seven decades ago [211], there is still a lively debate in the specialized literature on the nature of the active sites and on the oxidation state of the active chromium species [35, 51, 209, 212-231].

In a recent work, Groppo and co-workers [231] reported a detailed vibrational, electronic and structural investigation on the formation of the active sites in Cr^{VI}/SiO_2 based on the synergic use of *operando* Cr K-edge XANES (Fig. 3a), diffuse reflectance UV-Vis and Fourier-transform infra-red (FTIR) spectroscopies. The spectroscopic data were coupled with online mass spectrometry and supported by theoretical calculation (Fig. 3b and insets). The strength of the work consisted in the multi-technique approach that allowed the authors monitoring at the same time the changes

occurring at the Cr sites, the nature and location of the byproducts and the occurrence of ethylene polymerization (Fig. 3c).
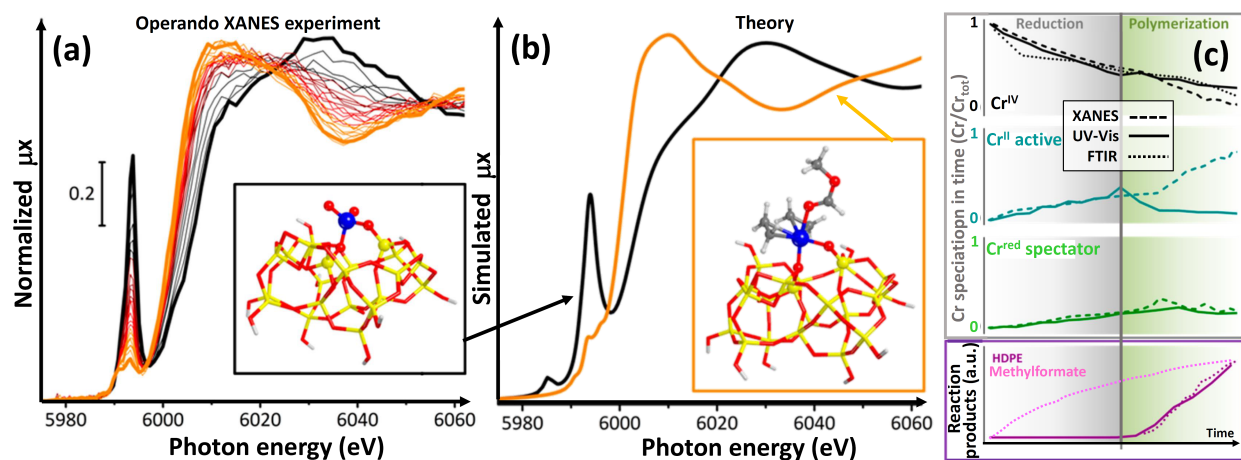

Fig. 3. Part (a): time evolution of the *operando* Cr K-edge XANES spectra of the Cr^{VI}/SiO_2 catalyst (bold black) during reduction with ethylene (from black to bold red) and during ethylene polymerization at 150 °C (from bold red to bold orange). Spectra were collected in fluorescence mode (see Fig. 1a) at the BM23 beamline of the ESRF [232]. Part (b): simulated XANES spectra, computed with the FSMNES code [37, 38], of Cr^{VI}/SiO_2 (black) and Cr^{II}/SiO_2 in interaction with methylformate and ethylene (orange), and corresponding structural models used to compute the XANES spectra (insets) , where silica support has a brutto formula of $Si_{21}O_{48}H_{10}$. Part (c): time-resolved spectroscopic speciation along the three *operando* experiments: XANES (dashed curves), UV−vis−NIR (solid curves) and FTIR (dotted curves). Spectroscopic fingerprints of, from top to bottom: Cr^{VI} (first component in the XANES PCA analysis; 21500 cm^{-1} UV-vis transition; and 1980 cm^{-1} FTIR band; Cr^{II} in interaction with methylformate and ethylene (third second component in the PCA XANES analysis; and 9500 cm^{-1} UV-vis transition; spectator Cr species (third component in the PCA XANES analysis; and 15100 cm^{-1} UV-vis transition); HDPE (4400−4050 cm^{-1} UV−vis transition; and 2853 cm^{-1} FTIR band) and methylformate (1573 cm^{-1} FTIR band). Adapted with permission from Ref. [231], copyright American Chemical Society, (2017).

XANES spectroscopy is the most appropriate technique to get quantitative structural information in the Cr species hosted on the Phillips catalyst. Indeed, the mostly used structural techniques cannot be applied here as the amorphous nature of the silica support prevents the use of diffraction-based methods, while the high dilution of the active species (1.0 Cr wt.% on SiO_2) prevents the collection of high signal to noise (S/N) EXAFS data up to high k-region (see the S/N ratio in the spectra reported in Fig. 3a), needed to perform an accurate analysis.

The simulation of the XANES spectrum of the starting chromate species (black curves in Fig. 3a,b) was straightforward as its local structure (tetrahedral-like Cr^{VI}, characterized by two Cr=O double bonds and by two Cr–O single bonds with the silica surface) is well known [208, 213, 217]. The spectrum obtained from the FDMNES [37, 38] simulation (black curve in Fig. 3b) on the chromate cluster optimized with Gaussian 9.0 code [149] (inset in Fig. 3a) perfectly reproduced all the features of the experimental spectrum (black curves in Fig. 3a).

The quantitative analysis of the remaining set of *operando* XANES spectra reported in Fig. 3a has been much more complex. The crucial key for the success of the study was the very careful tuning of the experimental parameters in the three *operando* experiments (XANES, UV-Vis and FTIR) that allowed Groppo and co-workers to clearly distinguish between the formation of the active sites (reduction of Cr^{VI} to Cr^{II}) and the beginning of the polymerization reaction. The series of spectra from the black to bold red spectrum in Fig. 3a refer to the $Cr^{VI} \rightarrow Cr^{II}$ reduction by ethylene. The XANES spectrum of the pure Cr^{II}/SiO_2 phase was obtained by reducing Cr^{VI}/SiO_2

with CO [213] and satisfactory simulated by Gianolio et al. [35] by using the previous version of the FDMNES code [119]. The correct insight to reproduce the final spectrum (bold orange curve in Fig. 3a), mainly representing the Cr^{II} sites in interaction with the by-product of the ethylene oxidation, came from the *operando* FTIR experiment showing the presence of two bands at 1617 and 1573 cm^{-1} (the latter very strong) that evolve in a parallel way and which were ascribed to the stretching modes of the O=C–O unit of methylformate adsorbed on Cr^{II} sites. On the basis of this observation, a cluster of Cr^{II}/SiO_2 in interaction with methylformate and ethylene was optimized with Gaussian 9.0 code [149] (inset in Fig. 3b) and used as input for the FDMNES [37, 38] to obtain the orange spectrum in Fig. 3b, that is able to well reproduce the main features of its experimental counterpart (bold orange curve in Fig. 3a).

The quantitative speciation for all the intermediate XANES spectra has been performed by MCR-ALS on the whole set of spectra reported in Fig. 3a, and resulted into three components [231]. The first component is virtually identical to the starting experimental spectrum (black curve in in Fig. 3a) and is consequently assigned to tetrahedral chromates in Cr^{VI}/SiO_2. The second component is a spectrum similar to that collected at the end of the reaction (bold orange curve in Fig. 3a), and is assigned to Cr^{II} in interaction with methylformate. Component 2 was recognized to be the active species in ethylene polymerization. Finally, component 3 is similar to component 2 in terms of edge position and white line contribution, while it differs in terms of pre-edge features. This spectrum is assigned to the Cr species defined from the UV-Vis measurements as the spectator ones [231]. Fig. 3c summarizes the quantitative speciation of both Cr species and products obtained by combining MCR-ALS analysis of the *operando* XANES spectra and the *operando* UV-Vis and FTIR studies.

Summarizing, Groppo and co-workers [231] have unraveled that the Cr sites involved in ethylene polymerization are divalent ions, 6-fold coordinated, and in interaction with an external nucleophilic methylformate ligand. This study provides the first spectroscopic identification, at the molecular level, of the oxygenated species adsorbed on the active Cr sites during the induction period of ethylene polymerization and introduce the important concept that oxygenates remain in the Cr coordination sphere during ethylene polymerization [231].

3.2. Ti sites in TS-1 catalyst: discrimination among different crystallographic sites

Titanium Silicalite-1 (TS-1) is a synthetic zeolite with MFI topology [233], where Ti atoms isomorphously substitute Si ones at tetrahedral (T) positions within the framework [31, 234-236] and is a highly selective industrial catalyst for partial oxidation reactions using H_2O_2 as oxidant [234, 237-244]. Because of the low concentration of tetrahedral Ti in the material (up to 3 wt% TiO_2 in the best cases), element selective (such as XAS [31, 80, 235, 236, 244-255] and XES [256, 257]), or chemical group selective (such as resonance Raman [244, 249, 253, 258-263]), techniques have been showed to be valuable tools toward its characterization. Even if TS-1 has been deeply investigated in the last 30 years, several fundamental aspects regarding its local structure are still open. In particular, the possible preferential substitution of Ti at certain specific crystallographic positions of the MFI framework is debated. The careful synchrotron X-ray powder diffraction study by Lamberti and coworkers inferred as Ti most probably sits in preferential framework positions, however the contrast between Ti and Si is insufficient to give a definitive picture [264]. The same authors later reported a neutron diffraction study in order to take advantage of the superior elemental contrast offered by this technique: the successful approach allowed to recognize sites T6, T7, T10 and T11 as the most probable for Ti substitution in TS-1 [265, 266].

A similar approach has been proposed by Hijar and coworkers [267] and Henry et al. [268], however both showing partly different outcomes.

Only recently, the possibility to exploit XANES as a tool for the location of Ti in the MFI framework has been proposed by Dong et al. [255], who based their work on a combined experimental-computational approach. In detail, they simulated Ti substitution at each of the 12 independent sites proper of the orthorhombic MFI framework with *Pnma* symmetry at periodic DFT level, then exploiting the resulting structural models as input for XANES simulation. By comparing the theoretical relative stabilities of the sites with experimental data (interpreted on the basis of the XANES simulations), they finally concluded as T4 is the most probable substitutional site for Ti.

Even if the last work presented a rigorous and valuable approach to the problem of Ti sitting position in TS-1, some aspects can be certainly improved. In a recent publication, Signorile et al. [269] reported a higher quality computational study of Ti substitution, both in terms of choice of the models and level of theory adopted (all electron, periodic B3LYP-D2 calculations). In detail, the MFI framework has been described by its lower monoclinic symmetry $P2_1n$ space group, since it has been demonstrated this polymorph is experimentally observed at low degrees of substitution (i.e. < 2 atoms per unit cell) of Si by Ti [234, 270]. This initial guess should guarantee a better description of a single substituted TS-1 (as usually assumed in computational studies), however paying the price of a doubled number (i.e. 24) of independent T sites to be considered (see Fig. 4a). Another critical point in the simulation of MFI zeolites is represented by the high flexibility of this framework, which leads to a rather complex potential energy surface, characterized by several local minima. In order to explore a wider portion of it, Signorile et al. [269] exploited multiple initial structures (also generated by low level methods) as input for the periodic DFT approach. Finally, the authors relaxed all the initial structures at high computational level with the CRYSTAL14 code [271], by exploiting the B3LYP-D functional and a double-ζ quality basis set. The most energetically stable model for each site have been exploited to generate a relative stabilities ranking for the Ti substitution: sites T10, T9 and T15 have been found to be the most stable, accounting for more of the 80% of the substituted positions. The models have been validated by simulating NH_3 adsorption and comparing the obtained energetic values with experimental ones [245, 246]. The key role of the inclusion of dispersive forces in the simulation of adsorptive processes in microporous materials has been carefully taken in account [272-275], finally leading to a very good agreement with calorimetric data [245, 246].

The DFT models described above [269] have been exploited for the XANES analysis of the spectrum of a well-manufactured TS-1 (i.e. containing only tetrahedral Ti sites), carefully dehydrated at 450°C [244]. The acquisition of the spectrum has been performed at XAFS beamline [276] of the Elettra synchrotron. We worked in transmission mode at the Ti K-edge (4984 eV) using a designed cell that allowed ex situ pre-treatment [277]. The XANES simulations have been carried on with FDMNES code [119, 120], that uses the finite difference method to solve the Schrödinger equation (see Section 2.1). The convolution function adopted to model the experimental broadening is an arctangent. The simulations have been performed by exploiting cluster models derived from the periodic simulations discussed above, accounting for the three most stable (T9, T10, T24) and the two less stable (T4 and T24) Ti substituted sites. The results of the XANES simulation are presented in Fig. 4b. The experimental spectrum shows an intense pre-edge (peak A, see Fig. 4b) due to the 1s → 3pd (or $A_1 \rightarrow T_2$) electronic transition that is associated with Ti in tetrahedral coordination [31, 235, 244, 247-249, 253]. All the simulations reproduce the pre-edge, however the spectrum of the T15 and T10 models manifest the signal at the correct

energy. The intensity of the pre-edge is well represented for all the Ti sites, apart from the T15 and T4 where it is overestimated. The other spectral features are properly recreated with a good agreement for all the models. The T15 model seems to reflect slightly better all the experimental details and their energy position, even though the intensities of signals A and B exceed the experimental ones. Summarizing, all the simulated XANES spectra reasonably describe the experimental TS-1 spectrum, thus it is difficult to categorically infer a preferential substitutional position for the Ti site. The most probable hypothesis is that the experimental spectrum is a combination of many of the Ti models, possibly with a slightly higher abundance of the T15 site.
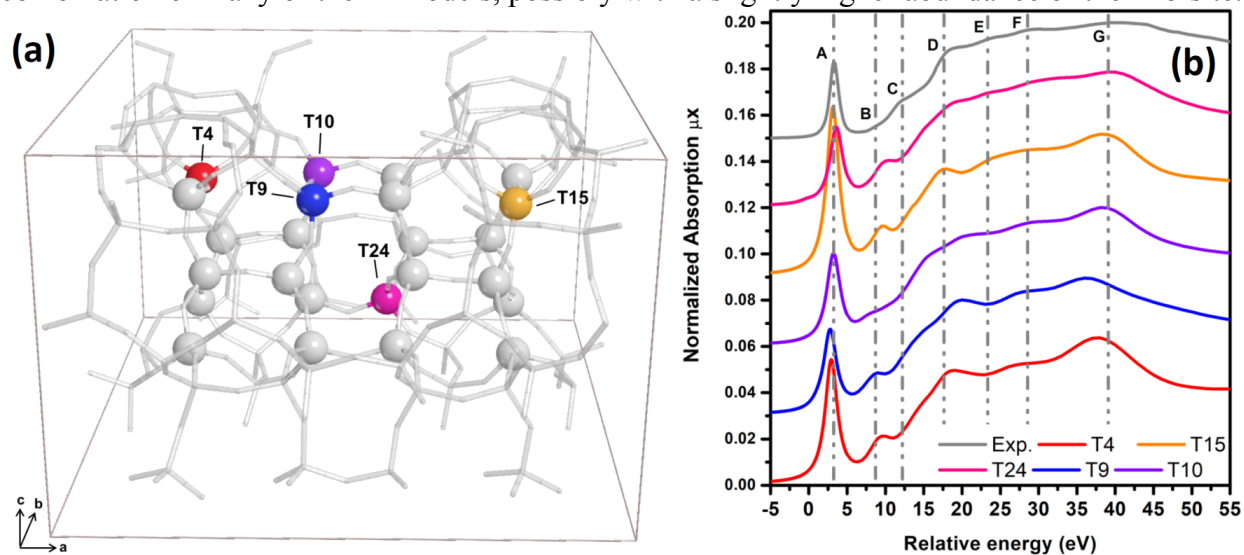

Fig. 4. Part (a): representation of the 24 independent T sites in the MFI unit cell in $P2_1/n$ symmetry. The sites, whose optimized structures have been exploited in XANES simulation (part b), are highlighted with colors: T4 (red), T9 (blue), T10 (violet), T15 (yellow) and T24 (fuchsia). Part (b): comparison among the experimental XANES spectrum at Ti K-edge of the TS-1 (gray) and the simulated spectra of five different Ti sites in the MFI framework: same color code as in panel (a). The energy alignment of the different spectra has been arbitrarily defined 80 eV below the minimum of the first EXAFS oscillation. This choice is consistent because the DFT optimized Ti–O first shell distances in the five investigated sites differ by less than 0.02 Å [244].

3.3. PdH_x and PdC_y stoichiometry determination of carbon supported Pd catalyst under ethylene hydrogenation reaction conditions

Formation of palladium hydride and carbide phases in the palladium-based catalysts is known to be critical for a number of important petrochemical reaction, such as catalytic hydrogenation of unsaturated hydrocarbons [278]. Under reaction conditions, the discrimination of palladium carbide and hydride phases is complicated due to the similar lattice parameters [279] of these two phases. In a series of previous works we have demonstrated that Pd K-edge XANES spectra are sensitive to the formation of palladium hydrides [279-288] and carbides [279, 283, 286-288], providing a new approach for *operando* characterization of the catalyst under reaction conditions by using hard X-rays.

The extraction of the quantitative information, such as the H/Pd loadings and the relative amount of the formed Pd-C bonds, can be performed by fitting the experimental difference XANES (ΔXANES) spectra by calculated ones. However, considering n independent structural parameters with the allowed ranges divided into N discrete values, the number of spectra to be calculated is given by N^n, which may lead to a considerable computational effort to cover the whole range. To reduce the number of calculated spectra, we applied the multidimensional interpolation

approach [289], as implemented in the FitIt code [290]. Fig. 5 shows the obtained dependencies of the theoretical ΔXANES spectra upon the increase of the interatomic Pd-Pd distances (part a), H/Pd (part b) and C/Pd ratios (part c). In each of the obtained $f(E,p)$ surfaces only few spectra (from 3 to 5) were explicitly calculated through the FDMNES code [37, 38], while the intermediate points were predicted by interpolation. To determine the minimal required order of the polynomial, the comparison of the directly calculated spectra with the interpolated ones have been performed. As an example, in the case of the different C/Pd ratio, a linear interpolation is appropriate in the C/Pd range from 0 to 0.125 (see Fig. 6).

The described approach allows the theoretical spectra to be constructed as a function of n parameters $f_{teor}(E,p_1,p_2,\ldots,p_n)$, which can be used to fit the experimental $f_{exp}(E_j)$ spectra by minimizing the difference $F(p_1,p_2,\ldots,p_n)$ between the experimental and theoretical spectra, being E_j the experimentally sampled energy points:

$$F(p_1, p_2, \ldots, p_n) \sim \sqrt{\Sigma_i \left[f_{teor}(E_i, p_1, p_2, \ldots, p_n) - f_{exp}(E_i) \right]^2} \qquad (3)$$

The obtained values of the interatomic parameters were found to be consistent with those determined by Fourier-analysis of EXAFS, and were successively fixed to the latter ones to reduce the number of variables in Eq. (3). The other two parameters, H/Pd and C/Pd ratios, provides important and complementary piece of information, inaccessible by standard EXAFS analysis.
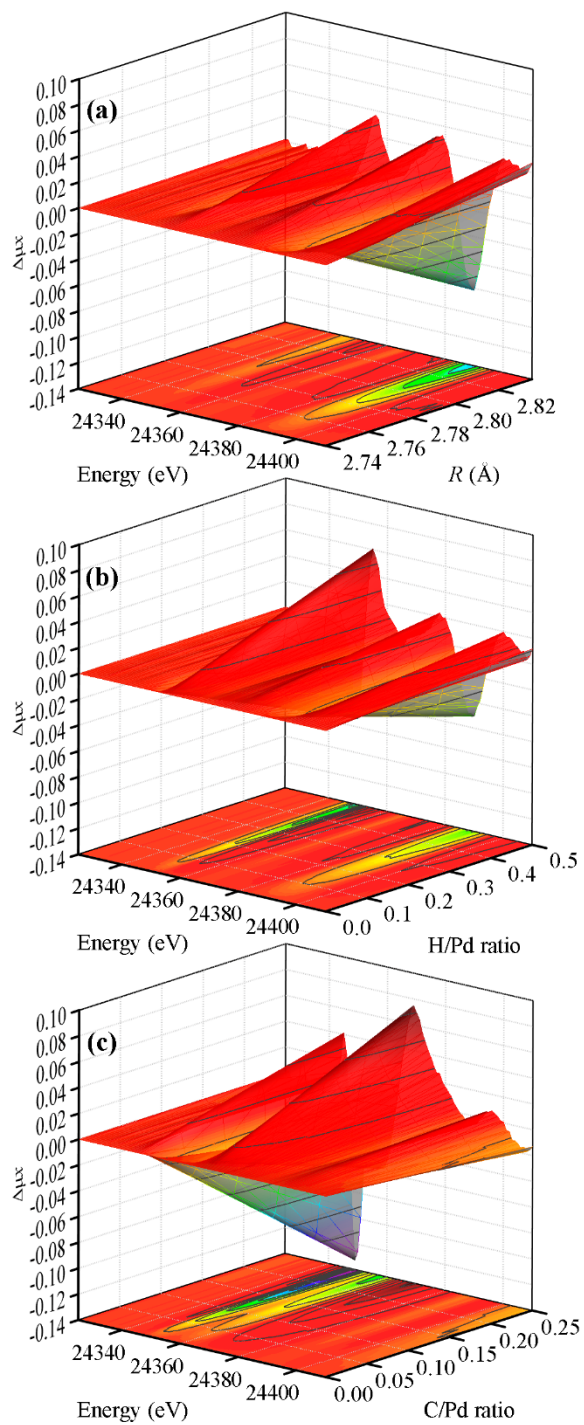
Fig. 5. Theoretical ΔXANES spectra demonstrating the effect of the increase of interatomic distances (a), H/Pd (b) and C/Pd (c) ratios.
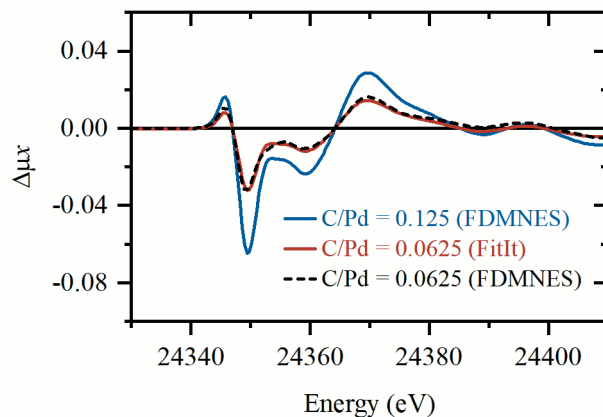
Fig. 6. Theoretical **Δ**XANES spectrum for a C/Pd ratio of 0.0625, obtained by linear interpolation (red line) between FDMNES-calculated spectra for bare Pd (horizontal black line) and PdC$_{0.125}$ (red line). The interpolated spectrum is compared with one directly calculated by FDMNES for the PdC$_{0.0625}$ model (dashed black line).

3.4. Copper site speciation in Cu-exchanged zeolites along thermal activation

This section is devoted to show the application of the MCR-ALS analysis (see Section 2.2) on a series of *operando* Cu K-edge XANES spectra collected on a Cu-exchanged chabasite (Cu-CHA) catalyst [291], that is currently object of intensive research efforts due its outstanding performance in deNO$_x$ chemistry [292-302] and its activity in the partial oxidation of methane to methanol (MTM) [303-305]. The understanding, at the atomic scale, the correlation between the catalyst composition and the nature of the Cu-species formed upon activation is fundamental to unleash the potential of this promising material. In previous works [188, 306], we applied the MCR approach, principally to the near-edge region (XANES), in order to quantitatively determine the spectroscopic signatures and the concentration profiles of the formed Cu-species.

We monitored by *in situ* XANES (at the BM23 beamline [232] of the ESRF synchrotron) the He activation, from room temperature (RT) to 400 °C, of a series of six Cu-CHA samples with Si/Al and Cu/Al ratio in the 5-29 and 0.1-0.6 ranges respectively [188]. Through this procedure, we tried to obtain a better spectroscopic contrast between the reducible and not reducible Cu-sites, gaining deeper insights in the self-reduction process in Cu-zeolites. The multivariate analysis (MCR-ALS) allowed us to single out the different XAS signatures of five pure Cu-species formed in the zeolite cages during the thermal treatment in inert gas: the results from this technique are summarized in Fig. 7. The pure XANES spectra and concentration retrieved from MCR-ALS (Fig. 7a,b) are in excellent agreement with our previous studies on Cu-CHA and with the report of Paolucci *et al.* [301]. Based on the spectroscopic fingerprints of each theoretical XANES spectrum and the correspondent temperature-dependent concentration profiles, we were able to assign each pure spectrum to a specific Cu moiety, Fig. 7c. Moreover, to reinforce these assignations, we simulated the Cu K-edge XANES spectra (see Section 2.1) for the proposed structures. Herein, the simulated XANES spectra properly reproduce the distinctive energy shifts of pure spectra and, even though partially, their intensity ratios. Detailed information on the XANES simulations can be found in ref. [188]. From MCR-ALS, several insights on the impact of the catalyst composition on Cu-speciation can be found. At RT, the formation of framework-interacting Cu-species from the mobile Cu(II) aquo-complexes seems to correlate with the appearance a four-coordinated Cu(II) dehydration intermediate, which abundance is maximum at around 130 °C (see Fig. 7b). Then, at higher temperatures, two species progressively develop, whose relative abundance

strongly correlates with the Si/Al ratio of the parent zeolite. These include: i) reduction-resistant Cu(II) species, charge-balanced by two proximal Al (named 2AlCu(II)), sitting in the chabazite six membered ring (6r); and ii) the redox-active 1Al[Cu(II)OH] complexes, preferentially located in the eight-membered ring (8r). The 2AlCu(II) population reach a plateau in the 200-300 °C range and remains stable until 400 °C. On the other hand, the highest 1Al[Cu(II)OH] concentration is observed at around 200 °C and therein start to progressively decrease in favor of the 1AlCu(I) one. These species are identified thanks to their typical Cu K-edge XANES features, i.e. the absence of the quadrupole $1s{\rightarrow}3d$ transition in the pre-edge region and the presence of a high intensity peak at ca. 8983 eV (commonly assigned to $1s{\rightarrow}4p$ transitions) in two- and three-fold coordinated Cu(I) centers [52, 62, 297, 307-309]. At 400 °C, the Cu-speciation can be described for all samples as a combination of 1Al[Cu(II)OH], 1AlCu(I) and 2AlCu(II) species. Furthermore, we independently validated these results by DFT-assisted, multi-component EXAFS fits. Remarkably, the high reducibility level observed in the low-loading sample (Cu/Al = 0.1) with Si/Al = 14 contrasts with the "2AlCu(II) saturation" scenario, currently dominating in the literature [82, 294, 297, 300, 310]. Moreover, the reducibility extend of 1Al[Cu(II)OH] complexes seems to depend on the Al distribution (the optimal reducibility is observed for Si/Al = 15). This evidence could be crucial to improve our understanding of the self-reduction process in Cu-zeolites, suggesting an important role of proximal Brønsted sites.
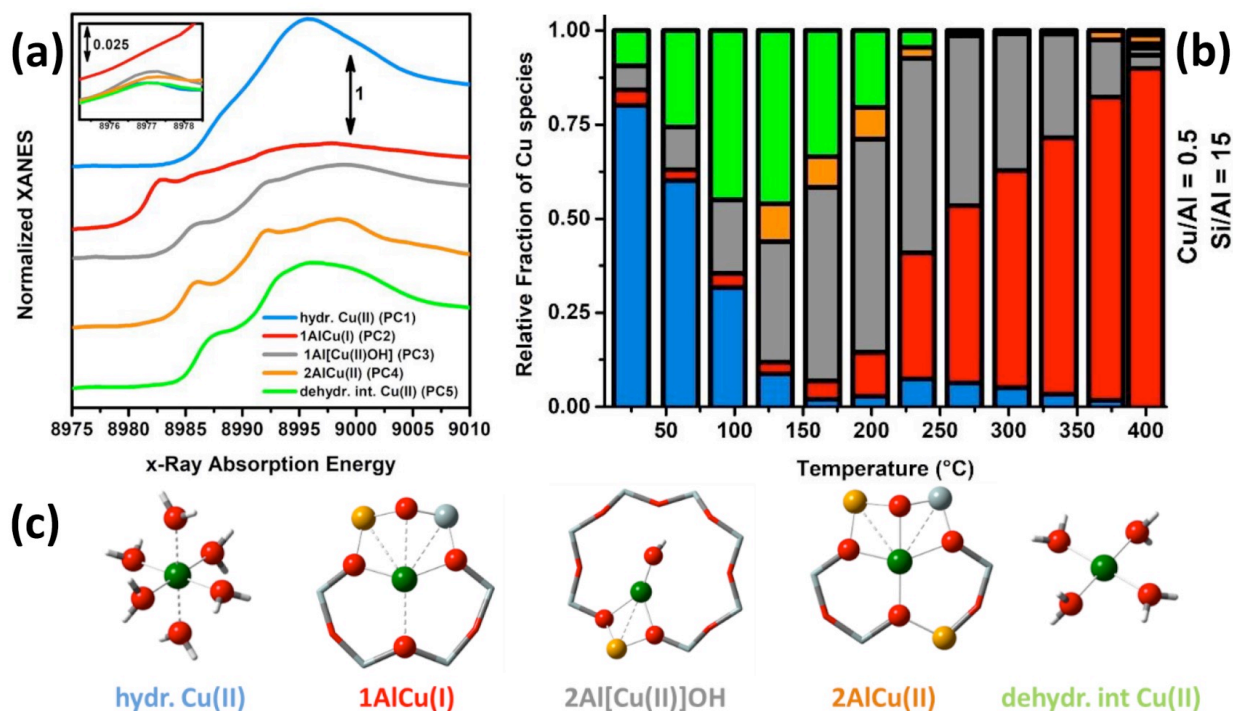

Fig. 7. (a) Results of MCR-ALS analysis of global temperature-dependent XANES dataset collected for six Cu-CHA samples with different compositions during He-activation from RT (25°C) to 400 °C. It has been assumed a common number of PCs equal to five. The inset reports a magnification of the quadrupolar Cu(II) 1s →3d transition. (b) Temperature dependent concentration profiles related to a selected sample with Cu/Al = 0.5 and Si/Al = 15 (bars follow the same color code of spectra in panel (a)). (c) Proposed assignments for the five pure components to specific Cu-moieties formed in the Cu-CHA catalyst during activation in inert flow. Atoms color code: Cu: green; H: white; O: red; Si: grey; Al: yellow.

As discussed in ref. [305], the availability of redox-active Cu-species, characterized by an efficient self-reduction process during thermal treatment, appears as a crucial requirement for the MTM conversion over Cu-CHA. Although 1Al[Cu(II)OH] sites are not directly active, they seem to represent the precursors for different Cu(II) active species, which formation requires high-temperature reaction with O_2. To shed light on this aspect, we focus on a selected Cu-CHA sample (Si/Al = 12, Cu/Al = 0.5), resulting in an optimal performance for the MTM process [305]. We performed a MCR analysis on HERFD XANES (ID26, ESRF) [88, 89, 311] data collected during different thermal treatments (in both He and O_2 gas flow, from RT to 500 °C), taking advantage of the superior energy resolution of the technique in the detection of O_2-derived Cu-species [306] (Fig. 8a). Herein, after the determination of the number of pure species through PCA (five for the activation in He and six for activation in O_2), we applied the ALS optimization (using six PCs) to a 'multi-way' column-wise augmented data matrix (see Fig. 8c) built joining two HERFD-XANES datasets collected during the two activations [306]. We pursued this choice because the datasets union largely increases the probability to find a pure spectrum whose concentration profile could not be fully imbedded into the concentration window of other components, making the spectral resolution process more effective [169]. Focusing on the He activation, the trend in the evolution of Cu moieties reported in Fig. 8d is qualitatively consistent with the one previously showed in Fig. 7b, where the concentration profile for a compositionally similar (Cu/Al=0.5 and Si/Al=15) sample has been reported. The decreasing of fully hydrated Cu(II) sites is strictly tied with the appearance of Cu(II) species, previously supposed to behave as dehydration intermediates. At higher temperatures the 1Al[Cu(II)OH] complexes (from ca. 170 °C inward) progressively form. Their concentration profile reaches a maximum at ca. 200 °C and then progressively decreases, in favor of reduced the 1AlCu(I) specie. 2AlCu(II) species appear from 200 °C and then reach a steady population after 400 °C (~ 15% of the mixture). The final state, as measured after 15 min in He at 500 °C, is dominated by a substantial fraction of reduced 1AlCu(I) sites, accounting for 51% of total Cu. Regarding the new component (*i.e.* PC4), in accordance with our previous work [188], it seems to play a marginal role in the signal reconstruction during the activation in He.
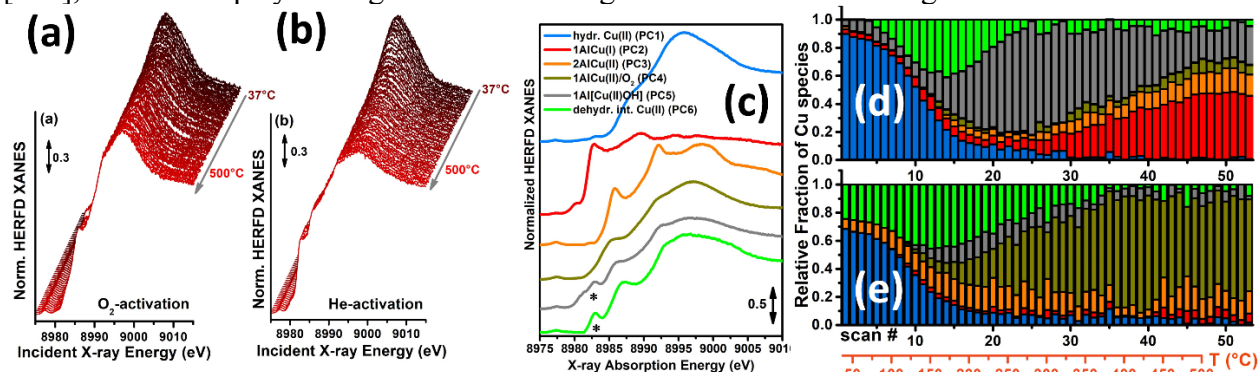

Fig. 8. Parts (a), (b): in situ temperature-dependent HERFD-XANES data collected during O_2- and He-activations, respectively, for Cu-CHA (Si/Al = 12, Cu/Al = 0.5). Part (c): pure spectra isolated through MCR-ALS algorithm of the in situ HERFD-XANES datasets reported in parts (a) and (b). The * symbol indicates the presence of reconstruction artefacts in the form of spurious rising-edge peaks for spectra PC5 and PC6. The cause of these results can be identified in the presence of very minor contributions, whose concentration profiles are completely embedded in the concentration window of much more abundant Cu species. (d), (e): concentration profiles for the pure HERFD-XANES spectra (reported in (c)) during He-activation (d) and O_2-activation (e), plotted as a function of the scan number (2 min/scan) and of the related data collection temperature (orange axis, from 37 °C to 500 °C, plus ~ 15 min dwelling time in isothermal conditions at 500 °C). Bars have the same colors as the corresponding spectra in panel (c).

As showed before, during the sample activation in O_2 the PC-space is higher than in He (six instead of five PCs). Herein, new concentration trends become evident (see Fig. 8e). After the typical dehydration phase, at ca. 150 °C, 1Al[Cu(II)OH] complexes and a new specie associated to the PC4 appear. Their XANES features are quite similar. This result suggests a similar Cu-coordination geometry for the two cases, indicating the nature of the PC4 as a Cu(II) site. It is worth noticing that, while 1Al[Cu(II)OH] species concentration tends to decrease during the activation, the concentration of the PC4 component progressively increases, becoming the dominant Cu component in the high-temperature range (70% total Cu at the end of the protocol). The 1AlCu(I) sites behave as minority specie, with a concentration oscillating between 2% and 5%. From these results, we can suppose that the new Cu(II) species could develop from the 1Al[Cu(OH)] sites (that act as a precursors) and through the re-oxidation process of Cu(I) species by O_2.

In order to understand the chemical nature of the corresponding O_2-derived Cu(II) sites, further studies and experiments should be performed especially in combination with XANES simulation of DFT-optimized structures for the different possible Cu_xO_y moieties [305, 312, 313]. In particular, the application of the MCR-ALS analysis on XANES spectra collected on different Cu-MOR samples of known activity allowed Pappas et al. to unambiguous determine the active site nuclearity of the direct methane to methanol conversion as a di-copper site.

3.5. Molecular adsorption at Ni^{2+} sites of CPO-27-Ni MOF

When the PCA analysis is performed on a series of experimental spectra the principal components are subject to a quantitative analysis. In the case of the Cr/SiO_2 polymerization catalyst reviewed in Section 3.1, describing the so-called fingerprint approach, DFT-optimized structures were used to calculate XANES and to compare them to the experimental data (Fig. 3). In Section 3.4, concerning the Cu red-ox chemistry in the Cu-CHA catalyst, the MCR-ALS approach has been applied to reconstruct, without any *a priori* guessed model, the XANES spectra of the principal components. These were attributed *a posteriori* to Cu species on the basis of an expected reaction path and, successively, the assignment was confirmed by comparing the XANES spectra attributed to pure phases and DFT computed spectra. This section deals with the deformations of the DFT optimized structure until the best agreement between the calculated and the experimental XANES spectrum is achieved. We have applied ML algorithms to perform a structural determination following both direct and indirect approaches.

The method is applied here to obtain the local structure of the Ni^{2+} adsorbing site hosted inside CPO-27-Ni MOF upon gas adsorption. While in the previous sections (3.1-3.4) we have chosen catalyst of industrial relevance, our choice for the last example concerns MOFs, a new class of porous crystalline materials that has attracted a huge attention in the scientific community [314-322]. Although the industrial application of MOFs is still limited to few cases [323], this new class of materials is predicted to play an important role in the next future, in the fields of gas storage and purification,[324-331], catalysis [332-343], electrocatalysis [344, 345] photocatalysis [346-349] and biocatalysis [350-357].

Gas sorption, separation and purification and catalytic applications require the availability of coordinatively unsaturated metal centers. CPO-27-Ni (also known as MOF-74, having $Ni_2(dhtp)(H_2O)_2 \cdot 8H_2O$ composition, where dhtp = 2,5-dihydroxyterephthalic acid), fulfills this request [358, 359]. CPO-27-Ni is a three-dimension honeycomb like framework with one-dimensional channels of about 11 Å diameter running along the *c* crystallographic axis (see Fig. 9a). At the intersections of the honeycomb are helical chains of cis-edge connected metal oxygen octahedra running along the [001] direction. The first coordination shell of Ni^{2+} sites consists of five framework oxygen atoms, while the sixth coordinative bond faces the channel and is available to coordinate ligand molecules, such as a water as shown in the inset in Fig. 9a. Several studies have investigated the adsorption of different probe molecules on the coordination vacancy of Ni^{2+} sites inside activated CPO-27-Ni MOFs, among them: H_2 [326, 360-362]; CH_4 [363, 364]: N_2 [365]; CO_2 [363, 366-368]; CO [168, 365, 368-370]; NO [371]; H_2O [372]; O_2 [373]; H_2S [168, 374]; thiophene [375]; dibenzothiophene [375].
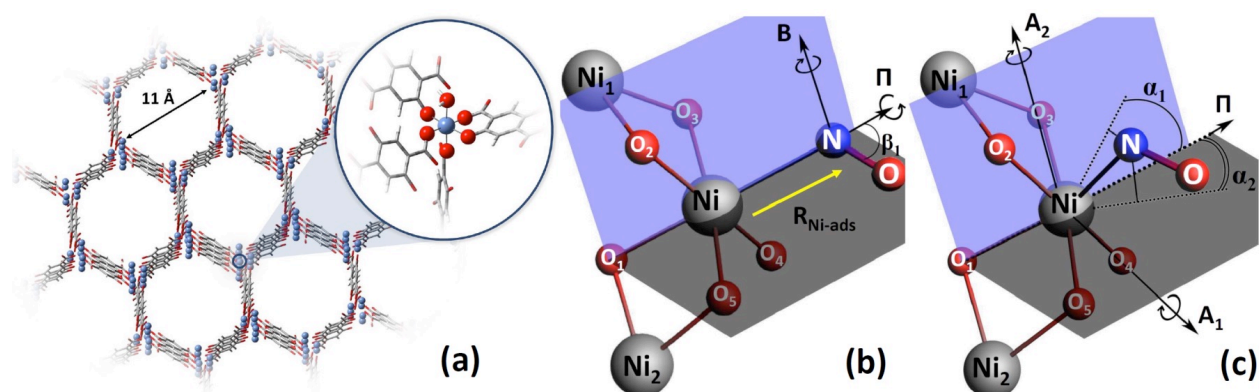

Fig. 9. Part (a): 3D representation of a dehydrated CPO-27-Ni structure, highlighting the honeycomb structure along the 1D channels of about 11 Å in diameter running along the [001] direction. The C atoms are reported in grey, H atoms in white, O in red, and Ni in blue. The inset reports a magnification of the first coordination spheres around a Ni^{2+} center (blue sphere) showing the five framework oxygen atoms (red spheres) and the coordination vacancy inside the channel saturated by a water molecule. Parts (b) and (c): structural parameters that were used for the refinement of the geometry of the adsorbed position relative to the Ni center in CPO-27-Ni MOF. The picture represents the NO adsorption case, but this can be straightforwardly extended to CO; the extension to CO_2 is made assuming (in first approximation) that the molecules remains linear upon adsorption. Taking atomic positions of the MOF framework from DFT calculations [168] the molecule is placed on the polar axis Π which passes through the Ni atom and O_1 atom from CPO-27-Ni framework. Two planes are then constructed: molecular plane, passing through Ni, N, O atoms (gray) and the perpendicular plane (blue). Four axes are used for the molecular rotations: the polar axis Π, the axis B (which passes through N perpendicularly to Π), the axis A_1 (which passes through Ni, perpendicularly to Π in molecular plane) and the A_2 axis (which passes through Ni, perpendicularly to Π in vertical plane). Any position of the molecule inside CPO-27-Ni framework is then constructed via successive transformations (order matters): the β_1 angle specifies then bending angle of the molecule relative to the polar axis; the β_2 angle specifies rotation of the molecule around the polar axis (β_2 is not shown in the figure for simplicity); the α_1 angle is the rotation of the whole adsorbate around A_1 and the α_2 angle is the rotation of the whole adsorbate around A_2. R_{Ni-ads} is the distance between Ni and closest atom of the adsorbed molecule.

The aim of the present study is to determine the structure of the NO, CO and CO_2 molecules adsorbed on Ni^{2+} sites of CPO-27-Ni, in terms of interaction distance and molecule orientation, by optimizing the structure dependent theoretical XANES spectra with the experimental ones. The

starting structures, used as input for the accelerated version of FDMNES [37, 38], have been those optimized in the periodic calculations performed with VASP5.3 code [376-378] using the PBE exchange-correlation potential [379] by Gallo et al. [168]. In this way, the deformation of the framework structure upon molecular adsorption are already included in the starting model. To optimize the adsorption geometry, the following parameters have been defined: the Ni-adsorbate distance (R_{Ni-ads}), two angles determining the position of the adsorbate molecule with respect to the Ni center (α_1, α_2) and two angles specifying the bending of the molecule (β_1, β_2), see Fig. 9b,c. The following fraction of the five dimensional space parameter has been investigated: $R^0_{Ni-ads} - \Delta R < R_{Ni-ads} < R^0_{Ni-ads} + \Delta R$; $-20° < \alpha_1, \alpha_2 < +20°$, $0 < \beta_1 < 90°$, while β_2 was unrestricted and free to vary in the whole [0° - 360°] interval. R^0_{Ni-ads} is the Ni-adsorbate distance optimized in the DFT calculations [168] and ΔR is fixed to 0.15 Å for CO and CO_2 (where there was a qualitative good agreement between theory [168, 316] and experiment [325, 369]) or to 0.25 Å for NO (because of a large disagreement between the DFT optimized value ($R_{Ni-ads} = 2.101$) [168, 372] and the value obtained from an EXAFS experiment ($R_{Ni-ads} = 1.87 \pm 0.02$) [371]). Note that the mostly used angle to define molecular adsorption (i.e. the Ni–N–O one [368]) in this notation is given by $180° - \beta_1$, see Fig. 9b. It is worth underlining that in this study we use difference XANES spectra for the analysis. The difference is calculated between spectrum measured in presence of adsorbate and that collected on the activated MOF, showing Ni^{2+} sites with a coordinative vacancy pointing toward the channel Fig. 9a. The use of difference spectra increases the sensitivity of fitting procedure and helps to avoid systematic errors of theoretical XANES spectra.

We use two different ML methods based on ridge regression and ensembles of random trees: Classical linear regression and Extra-Trees [193]. Classical linear regression uses the least squares method to build the best linear approximation for the target function; for example, dependency of XANES at a given energy point on the selected structural parameters (R_{Ni-ads}, α_1, α_2, β_1 and β_2) can be considered as a target function. The least squares method requires solution of the system of linear equations. In case of approximately linear dependent arguments this system is poorly defined. The addition to the matrix of the system of a unity matrix multiplied by a small value (ridge) helps to find stable solution.

The Extra-Trees [193] ML algorithm constructs a piecewise multilinear approximation of the target function. Tree form is used to represent the parameter-space, splitting it into several non-intersecting regions. Each region corresponds to a tree leaf, that contains a linear approximation of the target function. Functions of several randomized trees are averaged to produce the high-quality approximation. The Extra-Trees algorithm is fast and provides good quality outcomes, since it lacks of overfitting. Moreover, it is efficient for both small and large sample sizes [193]. To control the quality of the approximation of a function and to estimate the error bar for the predicted values, we apply a cross-validation.

We implemented two different approaches to define the structural parameters: the indirect method, described in Section 3.5.1 and the direct method, reported in Section 3.5.2. For both approaches the starting point is a set of calculated XANES spectra. A proper set of points, sampling homogeneously the region of structural parameters, is required in order to obtain a correct

approximation. A better approximation can be achieved via by using the improved Latin hypercube sampling (IHS). The comparison between a conventional grid sampling and IHS is shown in Fig. 10. As clear from Fig. 10b, the IHS is superior over grid sampling in terms of projected interpoint distance.
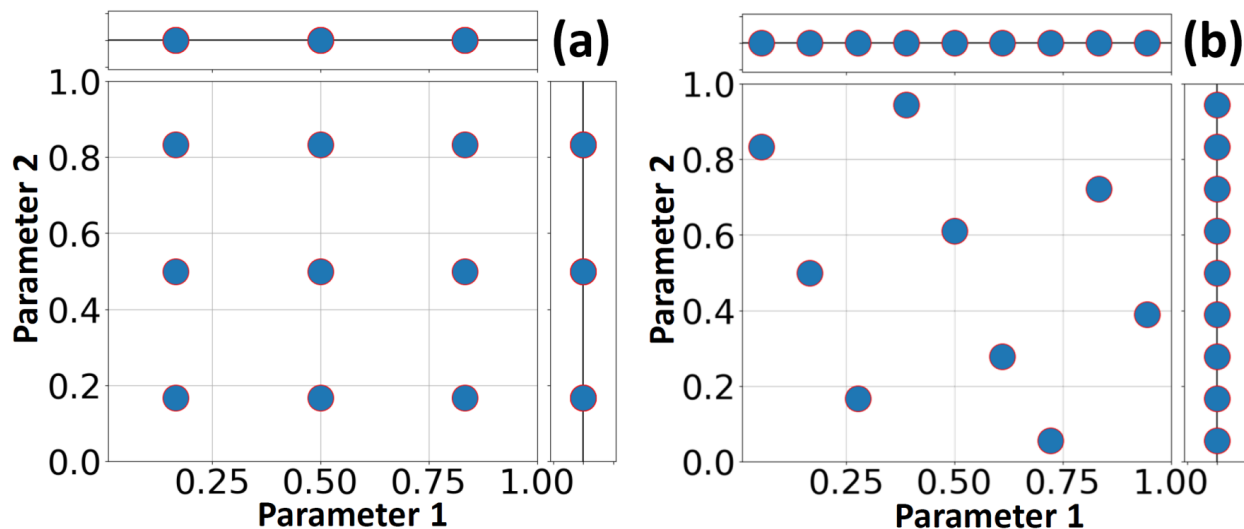

Fig. 10. Comparison between conventional grid (a) and IHS (b) sampling in a 2D space of parameters. While the total number of points is similar between the methods, the distance between projected points along different axes is smaller for IHS sampling. In our case we apply this scheme for a 5-dimension parameter space ($R_{Ni\text{-}ads}$, α_1, α_2, β_1 and β_2).

ML methods can be used for both direct and indirect approaches. These approaches use opposite choice of input parameters and target function. In the indirect approach, the ML algorithms are used to approximate XANES between different molecular geometries. The training dataset is used to establish correspondence geometry $\rightarrow$ XANES. The structural parameters are then used as input information for the algorithm, which predicts the XANES spectrum for the given parameters values. The approximated spectra are compared to the experimental one for different sets of structural parameters until the best agreement is obtained. The details of this procedure are described in Section 3.5.1. In the direct approach, the training dataset is used to establish the reciprocal correspondence: XANES $\rightarrow$ geometry. The input features for the ML algorithms are now the data points of XANES spectra. Once the algorithm is trained, the experimental spectrum is submitted as input and the corresponding geometry is predicted as the output of the process. A thoroughly discussion on the latter approach is given in section 3.5.2.

3.5.1. Indirect approach.

In general, the problem of the determination of the local structure from XANES spectrum requires *ab initio* computational programs, see Section 2.1. The algorithm searches the structure which provides the best matching between the theoretical and the experimental XANES spectra. Such procedure was first realized in the MXAN code [143-145, 380]. However, the minimization procedure requires a large number of accurate XANES calculations, being consequently very time

consuming. During the global minimum search, the optimization procedure should be repeated from many different starting points. Besides, every new experimental data for the same molecule should be analyzed separately repeating the protocol from the beginning.

The FitIt approach [289, 290] is based on the approximation of the XANES spectrum on the basis of a set of geometric parameters. This severely speeds up the optimization process but it requires preliminary calculations of XANES spectra for a given set of structural parameters. FitIt applies polynomial interpolation to approximate XANES. ML methods are superior for XANES approximation. In the present work, we use quadratic ridge regression and Extra-Trees for this purpose.

Hereafter, we describe step by step the procedure to apply the ML algorithms in the case of the indirect approach. In Fig. 9b,c we already defined the set of structural parameters to be determined. Fig. 11 shows the variation of XANES spectrum along the trajectory in the 5-dimensional space for the adsorption CO molecule over the open Ni^{2+} site of activated CPO-27-Ni.
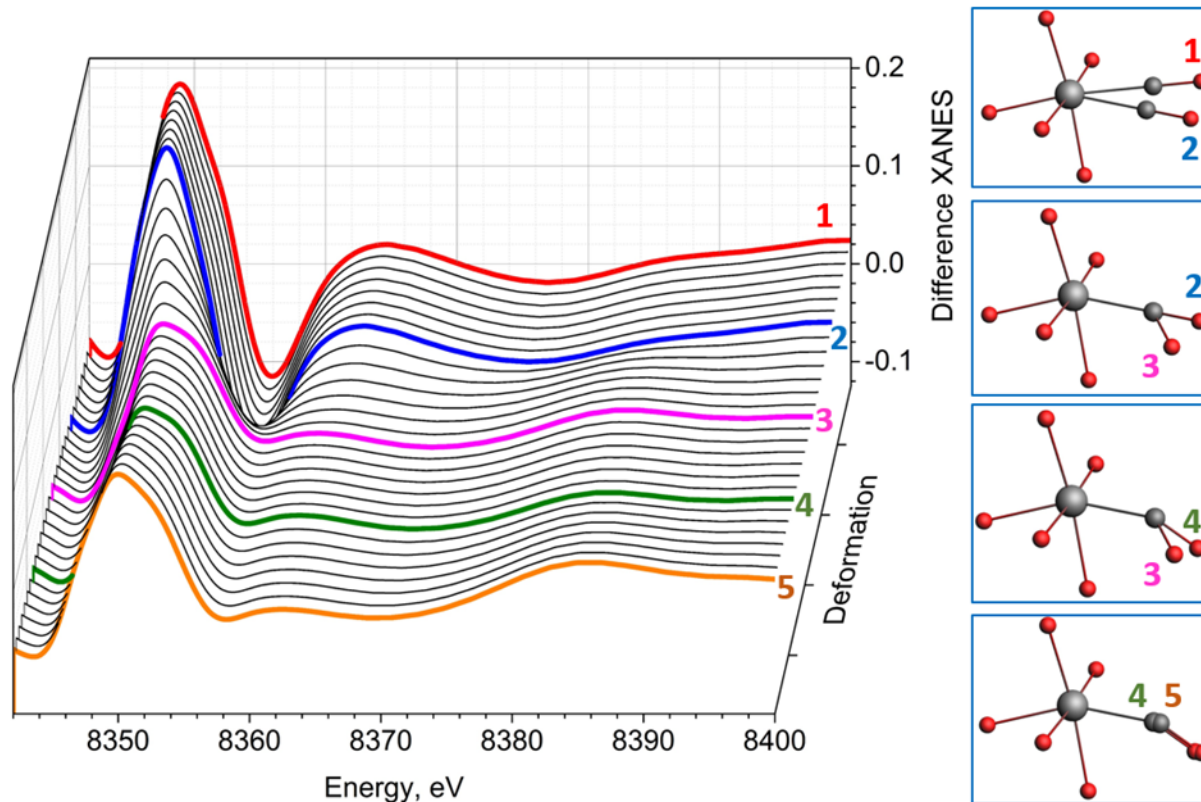

Fig. 11. Variation of the theoretical difference XANES spectra for the CPO-27-Ni/ CO adduct. The difference is calculated between spectra for the structure with adsorbed CO and that with naked Ni^{2+} (activated sample). The five bold colored curves correspond to the vertices of the trajectory in the 5-dimensional space [R_{ads}, α_1, α_2, β_1, β_2], from 1 to 5 :[2.0, 0.0, 0.0, 0.0, 0.0]; [2.0, 20.0, 0.0, 0.0, 0.0]; [2.0, 20.0, 0.0, 45.0, 0.0]; [2.0, 20.0, 0.0, 45.0, 90.0]; [2.15, 20.0, 0.0, 45.0, 90.0], respectively.

To estimate quantitatively the sensitivity of XANES to the variation of different parameters we used the relative standard deviation, as exemplified in Eq. (4) for the distance between Ni and gas (R_{Ni-ads}):

$$Std_{rel}(R_{Ni-ads}) = \frac{1}{E_2-E_1} \int_{E_1}^{E_2} \frac{\underset{\alpha 1,\alpha 2,\beta 1,\beta 2}{Mean} \left\{ \frac{Std}{R}[(XANES(R_{Ni-ads},\alpha_1,\alpha_2,\beta_1,\beta_2,E))] \right\}}{\underset{R,\alpha 1,\alpha 2,\beta 1,\beta 2}{Std}[(R_{Ni-ads},\alpha_1,\alpha_2,\beta_1,\beta_2,E)]} dE \qquad (4)$$

where XANES(R_{Ni-ads},α_1,α_2,β_1,β_2,E) is the XANES spectrum calculated for a given set of geometry parameters and energy E; the function $\underset{\alpha 1,\alpha 2,\beta 1,\beta 2}{Mean}\{...\}$ at the numerator is the averaged value of the standard deviation of the XANES spectrum obtained by changing only the R_{ads} parameter. This value is then normalized by the analogous standard deviation obtained by changing all parameters. This fraction is then integrated over all energy points of the XANES spectrum and normalized by the energy interval. $Std_{rel}(R_{Ni-ads})$ is the so-called mean influence of the parameter R_{Ni-ads} on the XANES spectrum. Equations analogous to Eq. (4) are used to define the mean influence of the remaining four parameters: $Std_{rel}(\alpha_1)$, $Std_{rel}(\alpha_2)$, $Std_{rel}(\beta_1)$ and $Std_{rel}(\beta_2)$. Table 2 reports the values of the mean influences for the five parameters and it allows determining quantitatively which parameters affect the XANES spectrum more.

Table 2. The relative standard deviation of XANES calculated as an effect of variation of different parameters on the spectrum. See details of the calculations in the text and equation (1)

Adsorbate	$Std_{rel}(R_{Ni-ads})$	$Std_{rel}(\alpha_1)$	$Std_{rel}(\alpha_2)$	$Std_{rel}(\beta_1)$	$Std_{rel}(\beta_2)$
CO	**0.69**	0.09	0.13	**0.69**	0.03
CO_2	**0.84**	0.10	0.20	**0.46**	0.03
NO	**0.77**	0.08	0.09	**0.58**	0.02

From the data summarized in Table 2 it clearly emerges that in all the three investigated cases (CO, CO_2 and NO) the distance between Ni^{2+} and the adsorbate (R_{Ni-ads}) and the bending angle (β_1) are the parameters that mainly influence XANES spectra. We will see further that the error of prediction of these parameters will be smaller than others in the direct approach.

The first step in the application of the indirect ML methods consists in the calculation of the theoretical training dataset of XANES spectra using finite difference method (FDMNES code [37, 38]) in the sampled points (see the grid in Fig. 10b) and in their convolution to account for the finite life time of the core hole. We used a sphere with a radius of 5.5 Å around the absorbing Ni atom and a 0.2 Å finite difference grid interpoint distance for the simulations (see Fig. 2b). The convolution parameters for the calculated spectra were obtained iteratively, by minimizing the discrepancy between experimental spectra and theoretical ones for the DFT optimized structures (details of the DFT optimization are described in [168]).

The ML algorithm is then trained on the basis of the calculated dataset. In order to estimate the quality of the XANES approximation, we further perform a cross-validation. In this step, we divide randomly the whole set of calculated spectra into 10 parts, then one of them is used successively as a validation test whereas the remining nine becomes the training set. The error value is then estimated as the ratio between the error of the average prediction and the error of the approximated spectrum. The average prediction is the averaged XANES spectrum over all geometric parameters. For the calculation of the error we use the L_2 norm factor, that is the integral over squared difference between theoretical and experimental difference spectra [193]. For 500 IHS points we approximate XANES at 0.16 and 0.20 relative to average prediction error for Extra-Trees and Ridge Regression algorithms correspondingly. The averaged L_2 norm over all 500 pairs of calculated by FDMNES and predicted spectra is 0.04 for Extra-Trees and 0.05 for Ridge Regression. In order to visualize these error values for a given approximated spectrum we sorted

all the pairs of difference between the exact and the predicted spectra by decay of their L_2 difference norm. Fig. 12 shows the pairs which correspond to the median error.
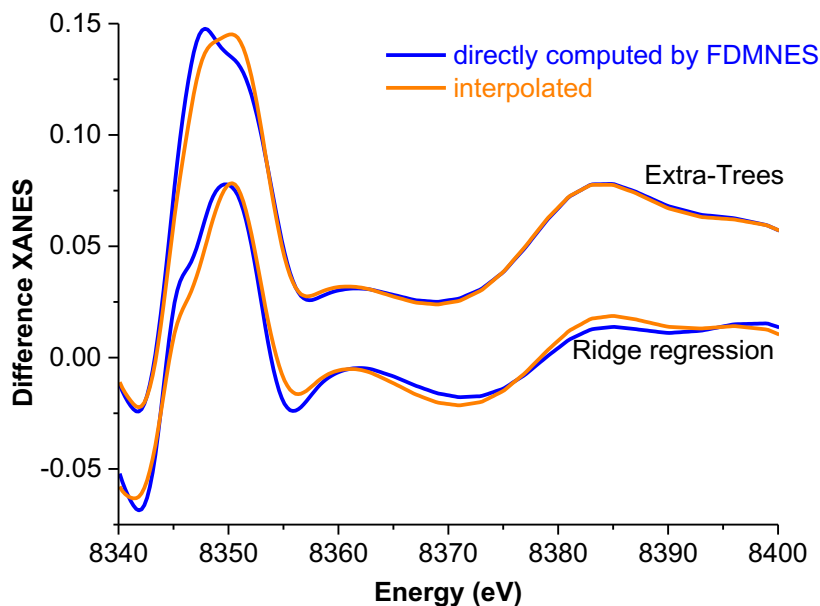

Fig. 12. Comparison between interpolated (orange) and exact (blue) difference XANES spectra for the CPO-27-Ni in interaction with CO, which differ from each other on the median error of interpolation. The difference spectra for Extra-Trees method were shifted vertically for clarity.

In case the quality of the approximation would not be satisfactory, one should increase number of IHS points (see Fig. 10b). In this case, a random sampling strategy is more convenient, since we can easily add new random points without recalculating all the sampling points as in IHS. Conversely, in case the quality of approximation would be considered satisfactory, we will perform the training of the ML algorithm on the whole set of calculated spectra and apply the optimization procedure to find the geometric parameters whose calculated spectrum fits best the experimental one in terms of L_2 norm. The amount of points required to achieve a good approximation depends on the range of variation of structural parameters. For the range of the parameter-space that has been investigated, we have determined that a value of IHS=500 (or random = 1000) gives as satisfactory interpolation. Table 3 and Fig. 13 summarize the structure prediction results obtained through the inverse method.

Table 3. Column labeled by (ML): structural parameters predicted by the ML inverse method for the CO, CO_2 and NO adsorption. For the two parameters for which ML analysis of XANES data is able to provide reliable estimations (R_{Ni-ads} and β_1), columns labeled with (DFT) give the comparison with the DFT optimized structures [168]. Finally, those labeled with (exp) give the comparison with the experimental values obtained by EXAFS [369, 371] or by with powder XRD refinement [325]. The solution for the case of NO adsorption was not unique and we obtained two minima with almost equal L_2 norm values between experimental and interpolated spectra. Single star (*) marks the minimum with larger Ni-N distance and linear configuration of the molecule; double stars (**) the second minimum with smaller Ni-N distance and bended configuration of the molecule.

Adsorbate	R_{Ni-ads} DFT (Å)	R_{Ni-ads} exp (Å)	R_{Ni-ads} ML (Å)	α_1 ML (°)	α_2 ML (°)	β_1-DFT (°)	β_1 exp (°)	β_1 ML (°)	β_2 ML (°)
CO	2.15	2.11(2) [a]	2.17	−3	−1	11	0 [a]	11	170
CO_2	2.38	2.289 [b]	2.30	6	−14	59	65(2) [b]	69	197
NO*	2.11	1.87(2) [c]	2.15	12	−11	58	50 [c]	25	290
NO**	2.11	1.87(2) [c]	1.97	9	3	58	50 [c]	70	359

[a] EXAFS data from ref. [369].
[b] Powder XRD data from ref. [325].
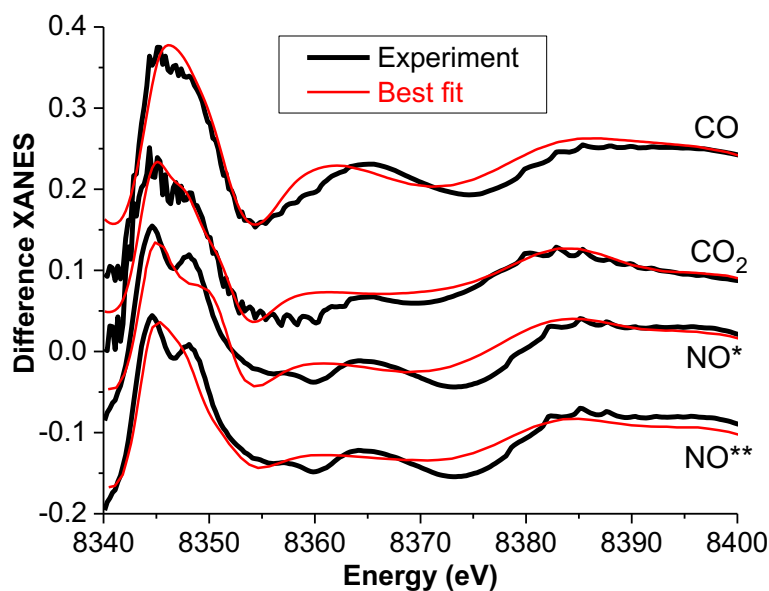[c] EXAFS data from ref. [371].

Fig. 13. Comparison between the best fit theoretical difference XANES spectra obtained with the ML approach (red curves) and experiment spectra (black curves) in terms of L_2 norm as obtained in the inverse method of fitting. Single star (*) marks the minimum with larger Ni-N distance and linear configuration of the molecule; double stars (**) mark the second minimum with smaller Ni-N distance and bended configuration of the molecule, see Table 3 for the structural details. The pairs of spectra for different molecules were shifted vertically for clarity.

In the case of CO adsorption the ML simulation provides a good agreement with both DFT and experimental values, being the discrepancies for R_{Ni-CO} of 0.02 and 0.06 Å, respectively and foreseens the end-on adsorption geometry ($\beta_1 = 11°$, corresponding to a Ni−C−O angle of 169°). Fig. 14 reports the two-dimensional L_2 norm distribution, showing the presence of a well-defined global minimum for the CO molecule, thus highlighting the reliability of the ML inverse method in determining both adsorption distance and Ni−C−O angle. The same holds for CO_2 adsorbate,

where the discrepancies with the experiment is 0.01 Å for R_{Ni-OCO} and 4° for β_1. More complex is the case of NO adsorbate. As described in Table 3, the solution for the NO adsorption is not unique. Two different geometrical configurations provide similar discrepancy between theory and experiment based on the integrated square difference, see Fig. 13.
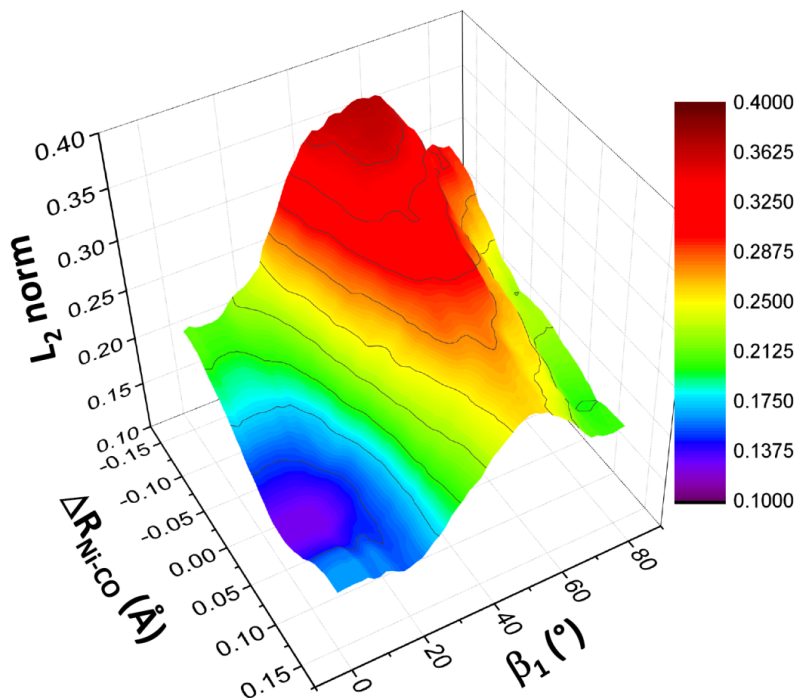

Fig. 14. L_2 norm calculated in the 2D subset of parameters from the 5D space for ML analysis of the XANES spectrum of CPO-27-Ni in interaction with CO. A clear minimum is observed for $\beta_1 = 11°$ and $\Delta R_{Ni-CO} = +0.02$ Å (with respect to the DFT optimized value, corresponding to $R_{Ni-CO} = 2.17$ Å, see Table 3), testifying that the ML inverse method is able to correctly define both adsorption distance and Ni−C−O angle. For symmetry reasons (see Fig. 9b) the L_2 norm values are symmetrical for the $\beta_1 \rightarrow -\beta_1$ operation (not shown in the figure.

3.5.2. Direct approach

The modern development of ML methods made it possible to apply a direct algorithm for solving a problem of finding of structural parameters. In contrast to the inverse approach, where the ML algorithms are used to predict the XANES spectral shape for a given set of structural parameters, in the direct approach ML algorithms are trained to predict the geometry parameters from a given XANES spectrum. The direct method has several advantages. First, this approach automatically divides the geometry parameters into two subsets: those which can be accurately determined from the XANES spectrum vs. those that cannot be precisely determined. Existing methods, based on minimizing the standard deviation from the experimental spectrum (MXAN [143-148] and FitIt [289, 290]), do not allow this discrimination. The second advantage is that there is no need to select the comparison metric of the XANES spectra. The minimization of different metrics leads to different final structures and it is not clear which is the correct one.

We found that for some geometry parameters the direct method of ML returns unstable results. Small changes of the properties of the algorithm (number of trees, depth of trees, etc.) or the change of the ML method cause large variations on the predicted values. Such behavior is not erroneous but intrinsic for geometry parameters with several possible values. In order to understand the reasons beyond this behavior, we estimated the probability of a parameter to belong to and an interval of values rather than predicting a single value.

To estimate the probability of the given parameter to be in a certain interval by means of Extra Trees, the task of direct prediction was reduced to the task of classification through a standard discretization procedure. The interval of the variation of structural parameter was divided into N equal segments $S_1 \ldots S_N$. The parameter value P has class *i* if P belongs to S_i. The results of training of Extra Trees classification algorithm over the XANES database and its application to the experimental spectrum of CO adsorbed on Ni^{2+} centers of CPO-27-Ni are the set of probabilities shown in Fig. 15.
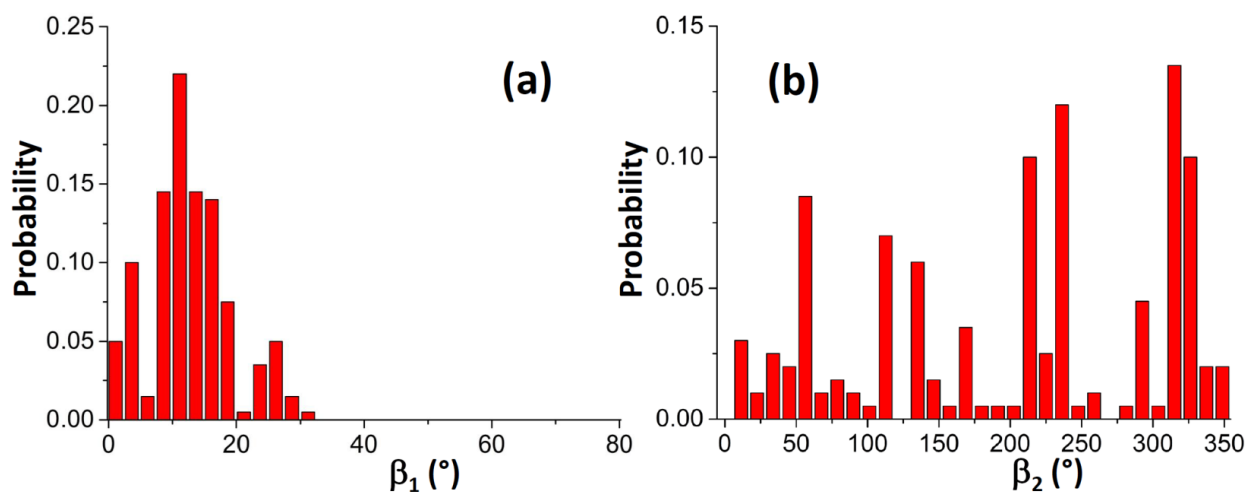

Fig. 15. Probability distribution predicted through the direct approach for the bending angle β_1 (part a) and rotation angle β_2 (part b) of the CO molecule relative to the Ni^{2+} center.

The results reported in Fig. 15 reflect outcomes of the the indirect ML approach (Table 2), where the high sensitivity of the XANES spectrum to the β_1 parameter ($Std_{rel}(\beta_1) = 0.69$) and a poor one for the β_2 ($Std_{rel}(\beta_2) = 0.03$) emerges. Indeed, the probability of finding β_1 has a narrow distribution around 10° (Fig. 15a), whereas the probability of finding β_2 is spread over the whole 0-360° range (Fig. 15b).

Table 4 shows the estimated parameters values (with the corresponding errors) obtained from the analysis of the XANES spectra with the ML direct method for CO, CO_2 and NO adsorption on CPO-27-Ni MOF. The cross-validation procedure, described above in section 3.5.1, is used to estimate the quality of the approximation in the geometry parameters (Error values in Table 4).

Table 4. Predicted values from direct approach and their mean average error calculated from the cross-validation procedure: columns labeled with (ML). For the two parameters for which ML analysis of XANES data is able to provide reliable estimations (R_{Ni-ads} and β_1), columns labeled with (DFT) give the comparison with the DFT optimized structures [168]. Finally, those labeled with (exp) give comparison with the experimental values obtained by EXAFS

[369, 371] or powder XRD refinements [325]. The solution for the NO absorption case was not unique. Single star (*) marks the minimum with larger Ni-N distance and linear configuration of the molecule; double stars (**) marks the second minimum with smaller Ni-N distance and bended configuration of the molecule.

Adsorbate	$R_{Ni\text{-}ads}$ DFT (Å)	$R_{Ni\text{-}ads}$ exp (Å)	$R_{Ni\text{-}ads}$ ML (Å)	α_1 ML (°)	α_2 ML (°)	β_1-DFT (°)	β_1 exp (°)	β_1 ML (°)	β_2 ML (°)
CO	2.15	2.11(2) [a]	2.14(1)	−5(8)	4(7)	11	0 [a]	13(3)	187(94)
CO_2	2.38	2.289 [b]	2.27(1)	1(8)	−8(5)	59	65(2) [b]	59(5)	209(91)
NO*	2.11	1.87(2) [c]	2.13(1)	−12(7)	−7(8)	58	50 [c]	25(4)	100(95)
NO**	2.11	1.87(2) [c]	2.03(1)	8(7)	8(8)	58	50 [c]	70(4)	260(95)

[a] EXAFS data from ref. [369].
[b] Powder XRD data from ref. [325].
[c] EXAFS data from ref. [371].

Summarizing, both the indirect (Table 2 and Table 3) and the direct (Table 4) ML approaches agree in highlighting that, among the 5 structural parameters selected in our study (Fig. 9b,c), only the adsorption distance ($R_{Ni\text{-}ads}$) and the bending angle β_1 affect significantly the XANES spectrum, and these can be reliably determined form the experiment. As far as $R_{Ni\text{-}ads}$ and β_1 parameters are concerned, both the indirect and the direct ML approaches provide quantitatively consistent values, that are in quantitative agreement with the experiments for the adsorption of CO and CO_2. Similarly to the results obtained in the inverse method, the probability distribution for the NO bending angle has two maxima, around 25° and 70°. The reason for this is intuitively clear from the Fig. 13, which shows the ambiguity in the positioning of the NO molecule with respect to the L_2 norm value. This fact can be attributed to the additional deformations of the CPO-27-Ni framework occurring upon adsorption and not properly accounted by DFT optimization. Thus, for a proper optimization of the NO adsorption geometry, the number of structural parameters should include some degrees of freedom for the CPO-27-Ni structure itself too, which we foresee to perform in future.

4. Conclusions and perspectives

As evidenced in the examples selected in this review, XANES spectroscopy has become a mature technique for the quantitative structural determination of active sites in the field of catalysis. Impressive improvements have been done in this direction since the early-eighties, when the semi-empirical Natoli's rule[381, 382] was formulated, correlating the energy position of the first XANES resonance after the edge with the inverse of the square of the first shell boned distance; nowadays a full 3D reconstruction of the local environment of the absorbing atom is achievable. Moreover, besides the intrinsic high penetration depth of hard X-rays that allow *operando* experiments to be performed in presence of reactants from both solid and liquid phases, the technique is pushing the frontier of science into two main directions.

The first direction concerns the improvements in the experimental setups, allowing spectra to be collected with progressively improved time- and/or spatial-resolution. Moreover, an increasing number of beamlines are presently (or will be soon) equipped with a secondary monochromator, allowing HERFD XANES spectra to be collected; this will improve the quality of the pre-edge, edge and post-edge features that can be detected, increasing the possibility to discriminate among structurally similar species. Another ongoing developments concerns XANES spectroscopy in the

soft X-ray range (200-1500 eV), sometime named near edge X-ray absorption fine structure (NEXAFS) [383-385], a potentially highly informative technique in the field of catalysis because it gives access to the L-edges of first-row transition metals and to the K-edges of relevant elements such (e.g. C, O and N). The former provide insight on the s-d-based unoccupied DOS, that is complementary to the p-based one investigated in K-edge XANES spectra with hard X-rays, the latter makes accessible insights from the reactants and products, that can complement the information on the metal active center. Unfortunately, for a long time, the low penetration depth of soft X-rays (and even the smaller of photoelectrons, when the electron yield-mode is chosen for detection) [94] has limited the studies in catalysis to *ex-situ* experiments. However, in the last years, instrumental improvements resulted in the realization of differential pumping systems [386, 387] and of membrane-based cells [388-390], where NEXAFS spectra (even in electron yield) can be collected under near-ambient and ambient pressures, respectively. We foresee that these instrumental improvements will represent a frontier in the studies of in situ and operando catalysts in the next few years.

The second direction is related to the data analysis and is twofold. On one hand, progressively more sophisticated codes allow a better reconstruction of the theoretical spectra, while the constant increase of the computational capabilities allows dealing with larger models in simulations and higher level of theory to be used in the solution of the Schrödinger equation. On the other hand, sophisticated approaches are used to handle the huge data sets generated by space- or by time-resolved experiments. Chemometric approaches such as PCA allow determining how many different species are contributing to the overall set of collected XANES spectra, while MCR-ALS approach, allows disentangling the XANES spectra of the pure species and to determine quantitatively their contribution in each of the different collected spectra. The application of ML approaches to XANES spectroscopy is still in its earlies stage but we foresee that it will revolutionize the way we are performing the XANES analysis and it will allow obtaining an unexpected number of structural information. The application of the advanced analytical tools described in this work is not restricted to XANES spectroscopy, but it can be in principle extended to any kind of spectroscopy, e.g. to X-ray emission spectroscopy (XES) [1, 88, 89, 311, 391], that is a complementary technique with respect to XANES allowing the occupied DOS to be investigated.

(Giovanni Agostini, Olivier Mathon and Sakura Pascarelli); ESRF BM31 beamline (Wouter van Beek, Hermann Emerich and Vladimir Dmitriev); Elettra XAFS beamline (Luca Olivi and Giuliana Aquilanti).

References

[1] J.A. van Bokhoven, C. Lamberti, X-Ray Absorption and X-Ray Emission Spectroscopy: Theory and Applications, John Wiley & Sons, Chichester (UK), 2016.
[2] H. Fricke, Phys. Rev., 16 (1920) 202-215.
[3] G. Hertz, Z. Phys., 3 (1920) 19-25.
[4] A.E. Lindh, Z. Phys., 6 (1921) 303-310.
[5] A. Lindh, E., Z. Phys., 31 (1925) 210-218.
[6] A.E. Lindh, Z. Phys., 63 (1930) 106-113.
[7] D. Coster, Z. Phys., 25 (1924) 83-98.
[8] D. Coster, J. Veldkamp, Z. Phys., 70 (1931) 306-316.
[9] D. Coster, J. Veldkamp, Z. Phys., 74 (1932) 191-208.
[10] K. Chamberlain, Phys. Rev., 26 (1925) 525-536.
[11] B.B. Ray, Z. Phys., 55 (1929) 119-126.
[12] D.M. Yost, Phil. Mag., 8 (1929) 845-847.
[13] B. Kievit, G.A. Lindsay, Phys. Rev., 36 (1930) 648-664.
[14] J.D. Hanawalt, Phys. Rev., 37 (1931) 715-726.
[15] J.D. Hanawalt, Z. Phys., 70 (1931) 293-305.
[16] A.S. Rao, K.R. Rao, Proc. Phys. Soc., 46 (1934) 163.
[17] L.V. Azaroff, Rev. Mod. Phys., 35 (1963) 1012-1021.
[18] D.E. Sayers, E.A. Stern, F.W. Lytle, Phys. Rev. Lett., 27 (1971) 1204-1207.
[19] F.W. Lytle, D.E. Sayers, E.A. Stern, Phys. Rev. B, 11 (1975) 4825-4835.
[20] E.A. Stern, D.E. Sayers, F.W. Lytle, Phys. Rev. B, 11 (1975) 4836-4846.
[21] N. Binsted, S.S. Hasnain, J. Synchrot. Radiat., 3 (1996) 185-196.
[22] J.J. Rehr, R.C. Albers, Rev. Mod. Phys., 72 (2000) 621-654.
[23] J.J. Kas, K. Jorissen, J.J. Rehr, Real-Space Multiple-Scattering Theory of X-Ray Spectra, in: J.A. van Bokhoven, C. Lamberti (Eds.) X-Ray Absorption and X-Ray Emission Spectroscopy: Theory and Applications, John Wiley & Sons, Chichester (UK), 2016, pp. 51-72.
[24] A. Filipponi, A. Dicicco, T.A. Tyson, C.R. Natoli, Solid State Commun., 78 (1991) 265-268.
[25] A. Filipponi, A. Di Cicco, C.R. Natoli, Phys. Rev. B, 52 (1995) 15122-15134.
[26] A. Filipponi, A. Di Cicco, Phys. Rev. B, 52 (1995) 15135-15149.
[27] C. Lamberti, J.A. van Bokhoven, Introduction: Historical Perspective on XAS, in: J.A. van Bokhoven, C. Lamberti (Eds.) X-Ray Absorption and X-Ray Emission Spectroscopy: Theory and Applications, John Wiley & Sons, Chichester (UK), 2016, pp. 3-21.
[28] A. Bianconi, Appl. Surf. Sci., 6 (1980) 392-418.
[29] R.A. Van Nordsthand, Adv. Catal., 12 (1960) 149-187.
[30] D. Li, G.M. Bancroft, M. Kasrai, M.E. Fleet, X.H. Feng, K.H. Tan, B.X. Yang, Solid State Commun., 87 (1993) 613-617.
[31] S. Bordiga, F. Boscherini, S. Coluccia, F. Genoni, C. Lamberti, G. Leofanti, L. Marchese, G. Petrini, G. Vlaic, A. Zecchina, Catal. Lett., 26 (1994) 195-208.
[32] S. Bordiga, R. Buzzoni, F. Geobaldo, C. Lamberti, E. Giamello, A. Zecchina, G. Leofanti, G. Petrini, G. Tozzola, G. Vlaic, J. Catal., 158 (1996) 486-501.
[33] A. Bianconi, J. Garcia, M. Benfatto, A. Marcelli, C.R. Natoli, M.F. Ruiz-Lopez, Phys. Rev. B, 43 (1991) 6885-6892.
[34] T.A. Tyson, K.O. Hodgson, C.R. Natoli, M. Benfatto, Phys. Rev. B, 46 (1992) 5997-6019.
[35] D. Gianolio, E. Groppo, J.G. Vitillo, A. Damin, S. Bordiga, A. Zecchina, C. Lamberti, Chem. Commun., 46 (2010) 976-978.
[36] E. Borfecchia, S. Maurelli, D. Gianolio, E. Groppo, M. Chiesa, F. Bonino, C. Lamberti, J. Phys. Chem. C, 116 (2012) 19839-19850.
[37] S.A. Guda, A.A. Guda, M.A. Soldatov, K.A. Lomachenko, A.L. Bugaev, C. Lamberti, W. Gawelda, C. Bressler, G. Smolentsev, A.V. Soldatov, Y. Joly, J. Chem. Theory Comput., 11 (2015) 4512-4521.

[38] A.A. Guda, S.A. Guda, M.A. Soldatov, K.A. Lomachenko, A.L. Bugaev, C. Lamberti, W. Gawelda, C. Bressler, G. Smolentsev, A.V. Soldatov, Y. Joly, J. Phys.: Conf. Ser., 712 (2016) 012004.

[39] L. Braglia, E. Borfecchia, L. Maddalena, S. Oien, K.A. Lomachenko, A.L. Bugaev, S. Bordiga, A.V. Soldatov, K.P. Lillerud, C. Lamberti, Catal. Today, 283 (2017) 89-103.

[40] L. Braglia, E. Borfecchia, K.A. Lomachenko, A.L. Bugaev, A.A. Guda, A.V. Soldatov, B.T.L. Bleken, S. Oien-Odegaard, U. Olsbye, K.P. Lillerud, S. Bordiga, G. Agostini, M. Manzoli, C. Lamberti, Faraday Discuss., 201 (2017) 277-298.

[41] Y. Tulchinsky, C.H. Hendon, K.A. Lomachenko, E. Borfecchia, B.C. Melot, M.R. Hudson, J.D. Tarver, M.D. Korzynski, A.W. Stubbs, J.J. Kagan, C. Lamberti, C.M. Brown, M. Dinca, J. Am. Chem. Soc., 139 (2017) 5992-5997.

[42] I.A. Pankin, A.A. Guda, N.A. Tumanov, Y. Filinchuk, K.A. Lomachenko, A.L. Bugaev, S.A. Guda, V.V. Shapovalov, C. Lamberti, A.V. Soldatov, J. Alloy. Compd., 735 (2018) 277-284.

[43] M.A. Soldatov, J. Göttlicher, S.P. Kubrin, A.A. Guda, T.A. Lastovina, A.L. Bugaev, Y.V. Rusalev, A.V. Soldatov, C. Lamberti, J. Phys. Chem. C, 122 (2018) 8543-8552.

[44] C.R. Natoli, M. Benfatto, S. Della Longa, K. Hatada, J. Synchrot. Radiat., 10 (2003) 26-42.

[45] J.J. Rehr, A.L. Ankudinov, Coord. Chem. Rev., 249 (2005) 131-140.

[46] L. Mino, G. Agostini, E. Borfecchia, D. Gianolio, A. Piovano, E. Gallo, C. Lamberti, J. Phys. D-Appl. Phys., 46 (2013) 423001.

[47] C. Garino, E. Borfecchia, R. Gobetto, J.A. van Bokhoven, C. Lamberti, Coord. Chem. Rev., 277 (2014) 130-186.

[48] Y. Joly, S. Grenier, Theory of X-Ray Absorption Near Edge Structure, in: J.A. van Bokhoven, C. Lamberti (Eds.) X-Ray Absorption and X-Ray Emission Spectroscopy: Theory and Applications, John Wiley & Sons, Chichester (UK), 2016, pp. 73-97.

[49] T. Tanaka, H. Yamashita, R. Tsuchitani, T. Funabiki, S. Yoshida, J. Chem. Soc.-Faraday Trans. I, 84 (1988) 2987-2999.

[50] H.C. Hu, I.E. Wachs, S.R. Bare, J. Phys. Chem., 99 (1995) 10897-10910.

[51] B.M. Weckhuysen, R.A. Schoonheydt, J.M. Jehng, I.E. Wachs, S.J. Cho, R. Ryoo, S. Kijlstra, E. Poels, J. Chem. Soc.-Faraday Trans., 91 (1995) 3245-3253.

[52] C. Lamberti, G. Spoto, D. Scarano, C. Paze, M. Salvalaggio, S. Bordiga, A. Zecchina, G.T. Palomino, F. Dacapito, Chem. Phys. Lett., 269 (1997) 500-508.

[53] C. Lamberti, S. Bordiga, A. Zecchina, M. Salvalaggio, F. Geobaldo, C.O. Arean, J. Chem. Soc.-Faraday Trans., 94 (1998) 1519-1525.

[54] V. Bolis, S. Maggiorini, L. Meda, F. D'Acapito, G.T. Palomino, S. Bordiga, C. Lamberti, J. Chem. Phys., 113 (2000) 9248-9261.

[55] C. Lamberti, G.T. Palomino, S. Bordiga, G. Berlier, F. D'Acapito, A. Zecchina, Angew. Chem.-Int. Edit., 39 (2000) 2138-2141.

[56] J.A. Rodriguez, T. Jirsak, J. Dvorak, S. Sambasivan, D. Fischer, J. Phys. Chem. B, 104 (2000) 319-328.

[57] M.Y. Sun, T. Burgi, R. Cattaneo, D. van Langeveld, R. Prins, J. Catal., 201 (2001) 258-269.

[58] A.L. Ankudinov, J.J. Rehr, J.J. Low, S.R. Bare, J. Chem. Phys., 116 (2002) 1911-1919.

[59] M. Fernandez-Garcia, Catal. Rev.-Sci. Eng., 44 (2002) 59-121.

[60] Y. Izumi, F. Kiyotaki, H. Yoshitake, K. Aika, T. Sugihara, T. Tatsumi, Y. Tanizawa, T. Shido, Y. Iwasawa, Chem. Commun., (2002) 2402-2403.

[61] C. Lamberti, C. Prestipino, F. Bonino, L. Capello, S. Bordiga, G. Spoto, A. Zecchina, S.D. Moreno, B. Cremaschi, M. Garilli, A. Marsella, D. Carmello, S. Vidotto, G. Leofanti, Angew. Chem.-Int. Edit., 41 (2002) 2341-2344.

[62] C. Prestipino, G. Berlier, F. Xamena, G. Spoto, S. Bordiga, A. Zecchina, G.T. Palomino, T. Yamamoto, C. Lamberti, Chem. Phys. Lett., 363 (2002) 389-396.

[63] D. Bazin, J.J. Rehr, J. Phys. Chem. B, 107 (2003) 12398-12402.

[64] C. Lamberti, S. Bordiga, F. Bonino, C. Prestipino, G. Berlier, L. Capello, F. D'Acapito, F. Xamena, A. Zecchina, Phys. Chem. Chem. Phys., 5 (2003) 4502-4509.

[65] M. Tromp, J.A. van Bokhoven, G.P.F. van Strijdonck, P. van Leeuwen, D.C. Koningsberger, D.E. Ramaker, J. Am. Chem. Soc., 127 (2005) 777-789.

[66] E. Bus, D.E. Ramaker, J.A. van Bokhoven, J. Am. Chem. Soc., 129 (2007) 8094-8102.

[67] G. Jacobs, Y.Y. Ji, B.H. Davis, D. Cronauer, A.J. Kropf, C.L. Marshall, Appl. Catal. A-Gen., 333 (2007) 177-191.

[68] E. Groppo, M.J. Uddin, S. Bordiga, A. Zecchina, C. Lamberti, Angew. Chem.-Int. Edit., 47 (2008) 9269-9273.

[69] S.T. Oyama, T. Gott, K. Asakura, S. Takakusagi, K. Miyazaki, Y. Koike, K.K. Bando, J. Catal., 268 (2009) 209-222.

[70] G. Smolentsev, G. Guilera, M. Tromp, S. Pascarelli, A.V. Soldatov, J. Chem. Phys., 130 (2009) 174508.

[71] Y.S. Chen, C. Xie, Y. Li, C.S. Song, T.B. Bolin, Phys. Chem. Chem. Phys., 12 (2010) 5707-5711.

[72] N.B. Muddada, U. Olsbye, L. Caccialupi, F. Cavani, G. Leofanti, D. Gianolio, S. Bordiga, C. Lamberti, Phys. Chem. Chem. Phys., 12 (2010) 5605-5618.

[73] D.E. Ramaker, D.C. Koningsberger, Phys. Chem. Chem. Phys., 12 (2010) 5514-5534.

[74] M. Ronning, N.E. Tsakoumis, A. Voronov, R.E. Johnsen, P. Norby, W. van Beek, O. Borg, E. Rytter, A. Holmen, Catal. Today, 155 (2010) 289-295.

[75] X.Y. Liu, A.Q. Wang, L. Li, T. Zhang, C.Y. Mou, J.F. Lee, J. Catal., 278 (2011) 288-296.

[76] C.V. Gaskell, C.M.A. Parlett, M.A. Newton, K. Wilson, A.F. Lee, ACS Catal., 2 (2012) 2242-2246.

[77] D. Gianolio, N.B. Muddada, U. Olsbye, C. Lamberti, Nucl. Instrum. Methods Phys. Res. Sect. B-Beam Interact. Mater. Atoms, 284 (2012) 53-57.

[78] C. He, G.H. Zhang, J. Ke, H. Zhang, J.T. Miller, A.J. Kropf, A.W. Lei, J. Am. Chem. Soc., 135 (2013) 488-493.

[79] A. Tougerti, E. Berrier, A.S. Mamede, C. La Fontaine, V. Briois, Y. Joly, E. Payen, J.F. Paul, S. Cristol, Angew. Chem.-Int. Edit., 52 (2013) 6440-6444.

[80] S. Bordiga, E. Groppo, G. Agostini, J.A. van Bokhoven, C. Lamberti, Chem. Rev., 113 (2013) 1736-1850.

[81] A. Boubnov, H.W.P. Carvalho, D.E. Doronkin, T. Gunter, E. Gallo, A.J. Atkins, C.R. Jacob, J.D. Grunwaldt, J. Am. Chem. Soc., 136 (2014) 13006-13015.

[82] F. Giordanino, E. Borfecchia, K.A. Lomachenko, A. Lazzarini, G. Agostini, E. Gallo, A.V. Soldatov, P. Beato, S. Bordiga, C. Lamberti, J. Phys. Chem. Lett., 5 (2014) 1552-1559.

[83] A. Gorczyca, V. Moizan, C. Chizallet, O. Proux, W. Del Net, E. Lahera, J.L. Hazemann, P. Raybaud, Y. Joly, Angew. Chem.-Int. Edit., 53 (2014) 12426-12429.

[84] S.Y. Yao, K. Mudiyanselage, W.Q. Xu, A.C. Johnston-Peck, J.C. Hanson, T.P. Wu, D. Stacchiola, J.A. Rodriguez, H.Y. Zhao, K.A. Beyer, K.W. Chapman, P.J. Chupas, A. Martinez-Arias, R. Si, T.B. Bolin, W.J. Liu, S.D. Senanayake, ACS Catal., 4 (2014) 1650-1661.

[85] C.W. Andersen, E. Borfecchia, M. Bremholm, M.R.V. Jorgensen, P.N.R. Vennestrom, C. Lamberti, L.F. Lundegaard, B.B. Iversen, Angew. Chem.-Int. Edit., 56 (2017) 10367-10372.

[86] A.W. Stubbs, L. Braglia, E. Borfecchia, R.J. Meyer, Y. Roman-Leshkov, C. Lamberti, M. Dinca, ACS Catal., 8 (2018) 596-601.

[87] K. Hamalainen, D.P. Siddons, J.B. Hastings, L.E. Berman, Phys. Rev. Lett., 67 (1991) 2850-2853.

[88] P. Glatzel, U. Bergmann, Coord. Chem. Rev., 249 (2005) 65-95.

[89] J. Singh, C. Lamberti, J.A. van Bokhoven, Chem. Soc. Rev., 39 (2010) 4754-4766.

[90] V.L. Aksenov, M.V. Koval'chuk, A.Y. Kuz'min, Y. Purans, S.I. Tyutyunnikov, Crystal. Rep., 51 (2006) 908-935.

[91] E. Fermi, Nuclear Physics, University of Chicago Press, Chicago, 1950.

[92] L.J. Brillson, Appendix 6: Derivation of Fermi's golden rule, in: Surfaces and Interfaces of Electronic Materials, Wiley-VCH Verlag GmbH & Co. KGaA, Weinheim, 2010, pp. 552-554.

[93] F. Boscherini, X-ray absorption fine structure in the study of semiconductor heterostructures and nanostructures, in: C. Lamberti, G. Agostini (Eds.) Characterization of Semiconductor Heterostructures and Nanostructures (2nd Edition), Elsevier, Amsterdam, 2013, pp. 259-310.

[94] E. Borfecchia, L. Mino, E. Groppo, S. Bordiga, A.L. Bugaev, A. Budnyk, K.A. Lomachenko, A.A. Guda, M.A. Soldatov, A.V. Soldatov, C. Lamberti, Stud. Surf. Sci. Catal., 177 (2017) 221-284.

[95] P.A.M. Dirac, Proc. Roy. Soc. (London) A, 114 (1927) 243-265.

[96] M. Steinmetz, S. Grimme, ChemistryOpen, 2 (2013) 115-124.

[97] A. Rosa, E.J. Baerends, S.J.A. van Gisbergen, E. van Lenthe, J.A. Groeneveld, J.G. Snijders, J. Am. Chem. Soc., 121 (1999) 10356-10365.

[98] E.J. Baerends, G. Ricciardi, A. Rosa, S.J.A. van Gisbergen, Coord. Chem. Rev., 230 (2002) 5-27.

[99] M. Stener, G. Fronzoni, M. de Simone, Chem. Phys. Lett., 373 (2003) 115-123.

[100] M.K. Nazeeruddin, F. De Angelis, S. Fantacci, A. Selloni, G. Viscardi, P. Liska, S. Ito, T. Bessho, M. Gratzel, J. Am. Chem. Soc., 127 (2005) 16835-16847.

[101] A.V. Luzanov, O.A. Zhikol, Int. J. Quantum Chem., 110 (2010) 902-924.

[102] L. Salassa, T. Ruiu, C. Garino, A.M. Pizarro, F. Bardelli, D. Gianolio, A. Westendorf, P.J. Bednarski, C. Lamberti, R. Gobetto, P.J. Sadler, Organometallics, 29 (2010) 6703-6710.

[103] A.R. Jaszewski, S. Petrie, R.J. Pace, R. Stranger, Chem.-Eur. J., 17 (2011) 5699-5713.

[104] E. Borfecchia, C. Garino, L. Salassa, T. Ruiu, D. Gianolio, X.Y. Zhang, K. Attenkofer, L.X. Chen, R. Gobetto, P.J. Sadler, C. Lamberti, Dalton Trans., 42 (2013) 6564-6571.

[105] F. de Groot, G. Vankó, P. Glatzel, J. Phys.: Condens. Matter, 21 (2009) 104207.

[106] F.d. Groot, Coord. Chem. Rev., 249 (2005) 31-63.

[107] E.L. Shirley, Phys. Rev. Lett., 80 (1998) 794-797.

[108] E.L. Shirley, J. Electron Spectrosc. Relat. Phenom., 144-147 (2005) 1187-1190.

[109] S. Sagmeister, C. Ambrosch-Draxl, Phys. Chem. Chem. Phys., 11 (2009) 4451-4457.

[110] J. Vinson, J.J. Rehr, J.J. Kas, E.L. Shirley, Phys. Rev. B, 83 (2011) 115106.

[111] K. Gilmore, J. Vinson, E.L. Shirley, D. Prendergast, C.D. Pemmaraju, J.J. Kas, F.D. Vila, J.J. Rehr, Comput. Phys. Commun., 197 (2015) 109-117.

[112] R.V. Pinjari, M.G. Delcey, M.Y. Guo, M. Odelius, M. Lundberg, J. Chem. Phys., 141 (2014) 124116.

[113] M. Guo, L.K. Sorensen, M.G. Delcey, R.V. Pinjari, M. Lundberg, Phys. Chem. Chem. Phys., 18 (2016) 3250-3259.

[114] K. Held, O.K. Andersen, M. Feldbacher, A. Yamasaki, Y.F. Yang, J. Phys.-Condes. Matter, 20 (2008) 064202.

[115] F. Aryasetiawan, O. Gunnarsson, Rep. Prog. Phys., 61 (1998) 237-312.

[116] D. Nabok, A. Gulans, C. Draxl, Phys. Rev. B, 94 (2016) 035118.

[117] G. Onida, L. Reining, A. Rubio, Rev. Mod. Phys., 74 (2002) 601-659.

[118] J.J. Rehr, J.J. Kas, M.P. Prange, A.P. Sorini, Y. Takimoto, F. Vila, Comptes Rendus Phys., 10 (2009) 548-559.

[119] Y. Joly, Phys. Rev. B, 63 (2001) 125120.

[120] Y. Joly, J. Synchrot. Radiat., 10 (2003) 58-63.

[121] C. Fonseca Guerra, J.G. Snijders, G. te Velde, E.J. Baerends, Theor. Chem. Acc., 99 (1998) 391-403.

[122] P. Giannozzi, S. Baroni, N. Bonini, M. Calandra, R. Car, C. Cavazzoni, D. Ceresoli, G.L. Chiarotti, M. Cococcioni, I. Dabo, A. Dal Corso, S. de Gironcoli, S. Fabris, G. Fratesi, R. Gebauer, U. Gerstmann, C. Gougoussis, A. Kokalj, M. Lazzeri, L. Martin-Samos, N. Marzari, F. Mauri, R. Mazzarello, S. Paolini, A. Pasquarello, L. Paulatto, C. Sbraccia, S. Scandolo, G. Sclauzero, A.P. Seitsonen, A. Smogunov, P. Umari, R.M. Wentzcovitch, J. Phys.-Condes. Matter, 21 (2009) 395502.

[123] S. Scandolo, P. Giannozzi, C. Cavazzoni, S. de Gironcoli, A. Pasquarello, S. Baroni, Z. Kristall., 220 (2005) 574-579.

[124] P. Giannozzi, C. Cavazzoni, Nuovo Cimento Soc. Ital. Fis. C-Colloq. Phys., 32 (2009) 49-52.

[125] T.A. Barnes, T. Kurth, P. Carrier, N. Wichmann, D. Prendergast, P.R.C. Kent, J. Deslippe, Comput. Phys. Commun., 214 (2017) 52-58.

[126] P. Giannozzi, O. Andreussi, T. Brumme, O. Bunau, M.B. Nardelli, M. Calandra, R. Car, C. Cavazzoni, D. Ceresoli, M. Cococcioni, N. Colonna, I. Carnimeo, A. Dal Corso, S. de Gironcoli, P. Delugas, R.A. DiStasio, A. Ferretti, A. Floris, G. Fratesi, G. Fugallo, R. Gebauer, U. Gerstmann, F. Giustino, T. Gorni, J. Jia, M. Kawamura, H.Y. Ko, A. Kokalj, E. Kucukbenli, M. Lazzeri, M. Marsili, N. Marzari, F. Mauri, N.L. Nguyen, H.V. Nguyen, A. Otero-de-la-Roza, L. Paulatto, S. Ponce, D. Rocca, R. Sabatini, B. Santra, M. Schlipf, A.P. Seitsonen, A. Smogunov, I. Timrov, T. Thonhauser, P. Umari, N. Vast, X. Wu, S. Baroni, J. Phys.-Condes. Matter, 29 (2017) 465901.

[127] M. Taillefumier, D. Cabaret, A.-M. Flank, F. Mauri, Phys. Rev. B, 66 (2002) 195107.

[128] C. Gougoussis, M. Calandra, A.P. Seitsonen, F. Mauri, Phys. Rev. B, 80 (2009) 075102.

[129] N.J. Vollmers, P. Müller, A. Hoffmann, S. Herres-Pawlis, M. Rohrmüller, W.G. Schmidt, U. Gerstmann, M. Bauer, Inorg. Chem., 55 (2016) 11694-11706.

[130] G. te Velde, F.M. Bickelhaupt, E.J. Baerends, C.F. Guerra, S.J.A. Van Gisbergen, J.G. Snijders, T. Ziegler, J. Comput. Chem., 22 (2001) 931-967.

[131] F. Neese, Wiley Interdiscip. Rev.-Comput. Mol. Sci., 2 (2012) 73-78.

[132] F. Neese, Wiley Interdiscip. Rev.-Comput. Mol. Sci., 8 (2018) e1327.

[133] C.J. Milne, T.J. Penfold, M. Chergui, Coord. Chem. Rev., 277-278 (2014) 44-68.

[134] P. Norman, A. Dreuw, Chem. Rev., 118 (2018) doi: 10.1021/acs.chemrev.1028b00156.

[135] J. Wenzel, M. Wormit, A. Dreuw, J. Chem. Theory Comput., 10 (2014) 4583-4598.

[136] D. Moonshiram, A. Guda, L. Kohler, A. Picon, S. Guda, C.S. Lehmann, X. Zhang, S.H. Southworth, K.L. Mulfort, J. Phys. Chem. C, 120 (2016) 20049-20057.

[137] D. Moonshiram, C. Gimbert-Suriñach, A. Guda, A. Picon, C.S. Lehmann, X. Zhang, G. Doumy, A.M. March, J. Benet-Buchholz, A. Soldatov, A. Llobet, S.H. Southworth, J. Am. Chem. Soc., 138 (2016) 10586-10596.

[138] J.J. Rehr, J.J. Kas, F.D. Vila, M.P. Prange, K. Jorissen, Phys. Chem. Chem. Phys., 12 (2010) 5503-5513.

[139] R.V. Vedrinskii, I.I. Gegusin, V.N. Datsyuk, A.A. Novakovich, V.L. Kraizman, Phys. Status Solidi B, 111 (1982) 433-442.

[140] V.N. Datsyuk, Gegusin, II, R.V. Vedrinskii, Phys. Status Solidi B-Basic Res., 134 (1986) 175-184.

[141] H. Ebert, Fully Relativistic Band Structure Calculations for Magnetic Solids - Formalism and Application, in: H. Dreyssé (Ed.) Electronic Structure and Physical Properties of Solids: the Users of the LMTO method, Springer, Berlin, 2000, pp. 191-246.

[142] H. Ebert, D. Kodderitzsch, J. Minar, Rep. Prog. Phys., 74 (2011) 096501.

[143] S. Della Longa, A. Arcovito, M. Girasole, J.L. Hazemann, M. Benfatto, Phys. Rev. Lett., 87 (2001) 155501.

[144] M. Benfatto, A. Congiu-Castellano, A. Daniele, S.D. Longa, J. Synchrot. Radiat., 8 (2001) 267-269.

[145] M. Benfatto, S. Della Longa, C.R. Natoli, J. Synchrot. Radiat., 10 (2003) 51-57.

[146] R. Sarangi, M. Benfatto, K. Hayakawa, L. Bubacco, E.I. Solomon, K.O. Hodgson, B. Hedman, Inorg. Chem., 44 (2005) 9652-9659.

[147] K. Hayakawa, K. Hatada, S. Della Longa, P. D'Angelo, M. Benfatto, AIP Conf. Proc., 882 (2007) 111-113.

[148] M. Benfatto, S. Della Longa, J. Phys.: Conf. Ser., 190 (2009) 012031.

[149] Gaussian 09, in: Gaussian 09, Revision A.02, M. J. Frisch, G. W. Trucks, H. B. Schlegel, G. E. Scuseria, M. A. Robb, J. R. Cheeseman, G. Scalmani, V. Barone, G. A. Petersson, H. Nakatsuji, X. Li, M. Caricato, A. Marenich, J. Bloino, B. G. Janesko, R. Gomperts, B. Mennucci, H. P. Hratchian, J. V. Ortiz, A. F. Izmaylov, J. L. Sonnenberg, D. Williams-Young, F. Ding, F. Lipparini, F. Egidi, J. Goings, B. Peng, A. Petrone, T. Henderson, D. Ranasinghe, V. G. Zakrzewski, J. Gao, N. Rega, G. Zheng, W. Liang, M. Hada, M. Ehara, K. Toyota, R. Fukuda, J. Hasegawa, M. Ishida, T. Nakajima, Y. Honda, O. Kitao, H. Nakai, T. Vreven, K. Throssell, J. A. Montgomery, Jr., J. E. Peralta, F. Ogliaro, M. Bearpark, J. J. Heyd, E. Brothers, K. N. Kudin, V. N. Staroverov, T. Keith, R. Kobayashi, J. Normand, K. Raghavachari, A. Rendell, J. C. Burant, S. S. Iyengar, J. Tomasi, M. Cossi, J. M. Millam, M. Klene, C. Adamo, R. Cammi, J. W. Ochterski, R. L. Martin, K. Morokuma, O. Farkas, J. B. Foresman, and D. J. Fox, Gaussian, Inc., Wallingford CT, 2016.

[150] K. Schwarz, P. Blaha, G.K.H. Madsen, Comput. Phys. Commun., 147 (2002) 71-76.

[151] K. Schwarz, P. Blaha, Comput. Mater. Sci., 28 (2003) 259-273.

[152] C. Hebert, J. Luitz, P. Schattschneider, Micron, 34 (2003) 219-225.

[153] K. Schwarz, J. Solid State Chem., 176 (2003) 319-328.

[154] C. Hebert, Micron, 38 (2007) 12-28.

[155] K. Schwarz, P. Blaha, S.B. Trickey, Mol. Phys., 108 (2010) 3147-3166.

[156] L. Pardini, V. Bellini, F. Manghi, C. Ambrosch-Draxl, Comput. Phys. Commun., 183 (2012) 628-636.

[157] M.W. Haverkort, M. Zwierzycki, O.K. Andersen, Phys. Rev. B, 85 (2012) 165113.

[158] A. Tanaka, T. Jo, J. Phys. Soc. Jpn., 63 (1994) 2788-2807.

[159] E. Stavitski, F.M.F. de Groot, Micron, 41 (2010) 687-694.

[160] G. Karlstrom, R. Lindh, P.A. Malmqvist, B.O. Roos, U. Ryde, V. Veryazov, P.O. Widmark, M. Cossi, B. Schimmelpfennig, P. Neogrady, L. Seijo, Comput. Mater. Sci., 28 (2003) 222-239.

[161] F. Aquilante, L. De Vico, N. Ferre, G. Ghigo, P.A. Malmqvist, P. Neogrady, T.B. Pedersen, M. Pitonak, M. Reiher, B.O. Roos, L. Serrano-Andres, M. Urban, V. Veryazov, R. Lindh, J. Comput. Chem., 31 (2010) 224-247.

[162] F. Aquilante, T.B. Pedersen, V. Veryazov, R. Lindh, Wiley Interdiscip. Rev.-Comput. Mol. Sci., 3 (2013) 143-149.

[163] F. Aquilante, J. Autschbach, R.K. Carlson, L.F. Chibotaru, M.G. Delcey, L. De Vico, I.F. Galvan, N. Ferre, L.M. Frutos, L. Gagliardi, M. Garavelli, A. Giussani, C.E. Hoyer, G. Li Manni, H. Lischka, D.X. Ma, P.A. Malmqvist, T. Muller, A. Nenov, M. Olivucci, T.B. Pedersen, D.L. Peng, F. Plasser, B. Pritchard, M. Reiher, I. Rivalta, I. Schapiro, J. Segarra-Marti, M. Stenrup, D.G. Truhlar, L. Ungur, A. Valentini, S. Vancoillie, V. Veryazov, V.P. Vysotskiy, O. Weingart, F. Zapata, R. Lindh, J. Comput. Chem., 37 (2016) 506-541.

[164] A. Gulans, S. Kontur, C. Meisenbichler, D. Nabok, P. Pavone, S. Rigamonti, S. Sagmeister, U. Werner, C. Draxl, J. Phys.-Condes. Matter, 26 (2014) 363202.

[165] C.K. Skylaris, P.D. Haynes, A.A. Mostofi, M.C. Payne, J. Chem. Phys., 122 (2005) 084119.

[166] J.C. Slater, Phys. Rev., 51 (1937) 846-851.

[167] T.A.W. Beale, R.D. Johnson, Y. Joly, S.R. Bland, P.D. Hatton, L. Bouchenoire, C. Mazzoli, D. Prabhakaran, A.T. Boothroyd, Phys. Rev. B, 82 (2010) 024105.

[168] E. Gallo, E. Gorelov, A.A. Guda, A.L. Bugaev, F. Bonino, E. Borfecchia, G. Ricchiardi, D. Gianolio, S. Chavan, C. Lamberti, Inorg. Chem., 56 (2017) 14408-14425.

[169] C. Ruckebusch, Resolving Spectral Mixtures: With Applications from Ultrafast Time-Resolved Spectroscopy to Super-Resolution Imaging, Elsevier, Amsterdam, 2016.

[170] R. Tauler, Chemometrics Intell. Lab. Syst., 30 (1995) 133-146.

[171] J. Jaumot, R. Gargallo, A. de Juan, R. Tauler, Chemometr. Intell. Lab., 76 (2005) 101-110.

[172] J. Jaumot, A. de Juan, R. Tauler, Chemometr. Intell. Lab., 140 (2015) 1-12.

[173] M. Fernandez Garcia, C.M. Alvarez, G.L. Haller, J. Phys. Chem., 99 (1995) 12565-12569.

[174] E.R. Malinowski, Factor analysis in chemistry, Wiley, New York, 2002.

[175] L. Braglia, E. Borfecchia, A. Martini, A.L. Bugaev, A.V. Soldatov, S. Oien-Odegaard, B.T. Lonstad-Bleken, U. Olsbye, K.P. Lillerud, K.A. Lomachenko, G. Agostini, M. Manzoli, C. Lamberti, Phys. Chem. Chem. Phys., 19 (2017) 27489-27507.

[176] M. Maeder, A. Zilian, Chemometrics Intell. Lab. Syst., 3 (1988) 205-213.

[177] W. Windig, J. Guilment, Anal. Chem., 63 (1991) 1425-1432.

[178] H. Abdollahi, R. Tauler, Chemometrics Intell. Lab. Syst., 108 (2011) 100-111.

[179] P. Conti, S. Zamponi, M. Giorgetti, M. Berrettoni, W.H. Smyrl, Anal. Chem., 82 (2010) 3629-3635.

[180] B.L. Caetano, V. Briois, S.H. Pulcinelli, F. Meneau, C.V. Santilli, J. Phys. Chem. C, 121 (2017) 886-895.

[181] H.W.P. Carvalho, S.H. Pulcinelli, C.V. Santilli, F. Leroux, F. Meneau, V. Briois, Chem. Mat., 25 (2013) 2855-2867.

[182] W.H. Cassinelli, L. Martins, A.R. Passos, S.H. Pulcinelli, C.V. Santilli, A. Rochet, V. Briois, Catal. Today, 229 (2014) 114-122.

[183] A. Voronov, A. Urakawa, W.v. Beek, N.E. Tsakoumis, H. Emerich, M. Rønning, Anal. Chim. Acta, 840 (2014) 20-27.

[184] J.P. Hong, E. Marceau, A.Y. Khodakov, L. Gaberova, A. Griboval-Constant, J.S. Girardon, C. La Fontaine, V. Briois, ACS Catal., 5 (2015) 1273-1282.

[185] A. Rochet, B. Baubet, V. Moizan, E. Devers, A. Hugon, C. Pichon, E. Payen, V. Briois, J. Phys. Chem. C, 121 (2017) 18544-18556.

[186] A.R. Passos, L. Martins, S.H. Pulcinelli, C.V. Santilli, V. Briois, ChemCatChem, 9 (2017) 3918-3929.

[187] N.E. Tsakoumis, J.C. Walmsley, M. Ronning, W. van Beek, E. Rytter, A. Hohnen, J. Am. Chem. Soc., 139 (2017) 3706-3715.

[188] A. Martini, E. Borfecchia, K.A. Lomachenko, I.A. Pankin, C. Negri, G. Berlier, P. Beato, H. Falsig, S. Bordiga, C. Lamberti, Chem. Sci., 8 (2017) 6836-6851.

[189] M.D. Dyar, E.A. Breves, M.E. Gunter, A. Lanzirotti, J.M. Tucker, C.J. Carey, S.E. Peel, E.B. Buown, R. Oberti, M. Lerotic, J.S. Delaney, Am. Mineral., 101 (2016) 1171-1189.

[190] E. Borfecchia, L. Mino, D. Gianolio, C. Groppo, N. Malaspina, G. Martinez-Criado, J.A. Sans, S. Poli, D. Castelli, C. Lamberti, J. Anal. At. Spectrom., 27 (2012) 1725-1733.

[191] L. Mino, E. Borfecchia, C. Groppo, D. Castelli, G. Martinez-Criado, R. Spiess, C. Lamberti, Catal. Today, 229 (2014) 72-79.

[192] L. Mino, E. Borfecchia, J. Segura-Ruiz, C. Giannini, G. Martinez-Criado, C. Lamberti, Rev. Mod. Phys., 90 (2018) 025007.

[193] T. Hastie, R. Tibshirani, J. Friedman, The elements of statistical learning. Data mining, inference, and prediction. (2nd Edition), Springer, New-York, 2009.

[194] X.H. Qu, D. Latino, J. Aires-de-Sousa, J. Cheminformatics, 5 (2013) 34.

[195] F. Pereira, K.X. Xiao, D. Latino, C.C. Wu, Q.Y. Zhang, J. Aires-de-Sousa, J. Chem Inf. Model., 57 (2017) 11-21.

[196] A.P. Bartok, M.J. Gillan, F.R. Manby, G. Csanyi, Phys. Rev. B, 88 (2013) 054104.

[197] J.R. Boes, J.R. Kitchin, Mol. Simul., 43 (2017) 346-354.

[198] F. Brockherde, L. Vogt, L. Li, M.E. Tuckerman, K. Burke, K.R. Muller, Nat. Commun., 8 (2017).

[199] I. Kruglov, O. Sergeev, A. Yanilkin, A.R. Oganov, Sci. Rep., 7 (2017) 8512.

[200] G. Hegde, R.C. Bowen, Sci. Rep., 7 (2017) 42669.

[201] J.P. Janet, L. Chan, H.J. Kulik, J. Phys. Chem. Lett., 9 (2018) 1064-1071.

[202] C. Zheng, K. Mathew, C. Chen, Y.M. Chen, H.M. Tang, A. Dozier, J.J. Kas, F.D. Vila, J.J. Rehr, L.F.J. Piper, K.A. Persson, S.P. Ong, npj Comput. Mater., 4 (2018) 12.

[203] J. Timoshenko, D.Y. Lu, Y.W. Lin, A.I. Frenkel, J. Phys. Chem. Lett., 8 (2017) 5091-5098.

[204] M. Weinstein, D. Horn, Phys. Rev. E, 80 (2009) 066117.

[205] M. Weinstein, F. Meirer, A. Hume, P. Sciau, G. Shaked, R. Hofstetter, E. Persi, A. Mehta, D. Horn, arXiv:1310.2700v2 [physics.data-an], (2013).

[206] World Polyethylene, in: World Polyethylene, Industry Study with Forecast for 2018 & 2023; The Freedonia Group: Cleveland, 2014; Study 3210.

[207] M.P. McDaniel, Adv. Catal., 33 (1985) 47-98.

[208] E. Groppo, C. Lamberti, S. Bordiga, G. Spoto, A. Zecchina, Chem. Rev., 105 (2005) 115-183.

[209] M.P. McDaniel, Adv. Catal., 53 (2010) 123-606.

[210] T.E. Nowlin, Business and Technology of the Global Polyethylene Industry, Wiley-Scrivener, New York, 2014.

[211] J.P. Hogan, R.L. Banks, Patent U.S. Patent 2, 825, 721, (1958).

[212] B.M. Weckhuysen, I.E. Wachs, R.A. Shoonheydt, Chem. Rev., 96 (1996) 3327-3349.

[213] E. Groppo, C. Prestipino, F. Cesano, F. Bonino, S. Bordiga, C. Lamberti, P.C. Thüne, J.W. Niemantsverdriet, A. Zecchina, J. Catal., 230 (2005) 98-108.

[214] E. Groppo, C. Lamberti, G. Spoto, S. Bordiga, G. Magnacca, A. Zecchina, J. Catal., 236 (2005) 233-244.

[215] E. Groppo, A. Damin, F. Bonino, A. Zecchina, S. Bordiga, C. Lamberti, Chem. Mater., 17 (2005) 2019-2027.

[216] E. Groppo, C. Lamberti, F. Cesano, A. Zecchina, Phys. Chem. Chem. Phys., 8 (2006) 2453-2456.

[217] G. Agostini, E. Groppo, S. Bordiga, A. Zecchina, C. Prestipino, F. D'Acapito, E. van Kimmenade, P.C. Thune, J.W. Niemantsverdriet, C. Lamberti, J. Phys. Chem. C, 111 (2007) 16437-16444.

[218] C.N. Nenu, E. Groppo, C. Lamberti, A.M. Beale, T. Visser, A. Zecchina, B.M. Weckhuysen, Angew. Chem.-Int. Edit., 46 (2007) 1465-1468.

[219] D.S. McGuinness, Chem. Rev., 111 (2011) 2321-2341.

[220] E. Groppo, K. Seenivasan, C. Barzan, Catal. Sci. Technol., 3 (2013) 858-878.

[221] M.P. Conley, M.F. Delley, G. Siddiqi, G. Lapadula, S. Norsic, V. Monteil, O.V. Safonova, C. Coperet, Angew. Chem.-Int. Edit., 53 (2014) 1872-1876.

[222] M.F. Delley, F. Nunez-Zarur, M.P. Conley, A. Comas-Vives, G. Siddiqi, S. Norsic, V. Monteil, O.V. Safonova, C. Coperet, Proc. Natl. Acad. Sci. U. S. A., 111 (2014) 11624-11629.

[223] C. Brown, J. Krzystek, R. Achey, A. Lita, R. Fu, R.W. Meulenberg, M. Polinski, N. Peek, Y. Wang, L.J.V. de Burgt, S. Profeta, A.E. Stiegman, S.L. Scott, ACS Catal., 5 (2015) 5574-5583.

[224] A. Chakrabarti, I.E. Wachs, Catal. Lett., 145 (2015) 985-994.

[225] D. Cicmil, J. Meeuwissen, A. Vantomme, J. Wang, I.K. van Ravenhorst, H.E. van der Bij, A. Munoz-Murillo, B.M. Weckhuysen, Angew. Chem.-Int. Edit., 54 (2015) 13073-13079.

[226] B. Peters, S.L. Scott, A. Fong, Y.H. Wang, A.E. Stiegman, Proc. Natl. Acad. Sci. U. S. A., 112 (2015) E4160-E4161.

[227] A. Chakrabarti, M. Gierada, J. Handzlik, I.E. Wachs, Top. Catal., 59 (2016) 725-739.

[228] D. Cicmil, J. Meeuwissen, A. Vantomme, B.M. Weckhuysen, ChemCatChem, 8 (2016) 1937-1944.

[229] D. Cicmil, I.K. van Ravenhorst, J. Meeuwissen, A. Vantomme, B.M. Weckhuysen, Catal. Sci. Technol., 6 (2016) 731-743.

[230] M.F. Delley, G. Lapadula, F. Nunez-Zarur, A. Comas-Vives, V. Kalendra, G. Jeschke, D. Baabe, M.D. Walter, A.J. Rossini, A. Lesage, L. Emsley, O. Maury, C. Coperet, J. Am. Chem. Soc., 139 (2017) 8855-8867.

[231] C. Barzan, A. Piovano, L. Braglia, G.A. Martino, C. Lamberti, S. Bordiga, E. Groppo, J. Am. Chem. Soc., 139 (2017) 17064-17073.

[232] O. Mathon, A. Beteva, J. Borrel, D. Bugnazet, S. Gatla, R. Hino, I. Kantor, T. Mairs, M. Munoz, S. Pasternak, F. Perrin, S. Pascarelli, J. Synchrot. Radiat., 22 (2015) 1548-1554.

[233] M. Taramasso, G. Perego, B. Notari, Patent US Patent No. 4410501, (1983).

[234] R. Millini, E. Previde Massara, G. Perego, G. Bellussi, J. Catal., 137 (1992) 497-503.

[235] S. Bordiga, S. Coluccia, C. Lamberti, L. Marchese, A. Zecchina, F. Boscherini, F. Buffa, F. Genoni, G. Leofanti, G. Petrini, G. Vlaic, J. Phys. Chem., 98 (1994) 4125-4132.

[236] C. Lamberti, S. Bordiga, D. Arduino, A. Zecchina, F. Geobaldo, G. Spano, F. Genoni, G. Petrini, A. Carati, F. Villain, G. Vlaic, J. Phys. Chem. B, 102 (1998) 6382-6390.

[237] G. Bellussi, A. Carati, M.G. Clerici, G. Maddinelli, R. Millini, J. Catal., 133 (1992) 220-230.

[238] F. Maspero, U. Romano, J. Catal., 146 (1994) 476-482.

[239] S.B. Kumar, S.P. Mirajkar, G.C.G. Pais, P. Kumar, R. Kumar, J. Catal., 156 (1995) 163-166.

[240] B. Notari, Microporous crystalline titanium silicates, in: D.D. Eley, W.O. Haag, B. Gates (Eds.) Advances in Catalysis, Vol 41, Elsevier Academic Press Inc, San Diego, 1996, pp. 253-334.

[241] W.B. Fan, R.G. Duan, T. Yokoi, P. Wu, Y. Kubota, T. Tatsumi, J. Am. Chem. Soc., 130 (2008) 10150-10164.

[242] L.H. Chen, X.Y. Li, G. Tian, Y. Li, J.C. Rooke, G.S. Zhu, S.L. Qiu, X.Y. Yang, B.L. Su, Angew. Chem.-Int. Edit., 50 (2011) 11156-11161.

[243] T.L. Lu, J.P. Zou, Y.Z. Zhan, X.M. Yang, Y.Q. Wen, X.Y. Wang, L.P. Zhou, J. Xu, ACS Catal., 8 (2018) 1287-1296.

[244] M. Signorile, V. Crocella, A. Damin, B. Rossi, C. Lamberti, F. Bonino, S. Bordiga, J. Phys. Chem. C, 122 (2018) 9021-9034.

[245] V. Bolis, S. Bordiga, C. Lamberti, A. Zecchina, A. Carati, F. Rivetti, G. Spano, G. Petrini, Langmuir, 15 (1999) 5753-5764.

[246] V. Bolis, S. Bordiga, C. Lamberti, A. Zecchina, A. Carati, F. Rivetti, G. Spano, G. Petrini, Microporous Mesoporous Mat., 30 (1999) 67-76.

[247] R.J. Davis, Z. Liu, J.E. Tabora, W.S. Wieland, Catal. Lett., 34 (1995) 101-113.

[248] D. Gleeson, G. Sankar, C.R.A. Catlow, J.M. Thomas, G. Spano, S. Bordiga, A. Zecchina, C. Lamberti, Phys. Chem. Chem. Phys., 2 (2000) 4812-4817.

[249] G. Ricchiardi, A. Damin, S. Bordiga, C. Lamberti, G. Spano, F. Rivetti, A. Zecchina, J. Am. Chem. Soc., 123 (2001) 11409-11419.

[250] S. Bordiga, A. Damin, F. Bonino, A. Zecchina, G. Spano, F. Rivetti, V. Bolis, C. Prestipino, C. Lamberti, J. Phys. Chem. B, 106 (2002) 9892-9905.

[251] A. Zecchina, S. Bordiga, G. Spoto, A. Damin, G. Berlier, F. Bonino, C. Prestipino, C. Lamberti, Top. Catal., 21 (2002) 67-78.

[252] F. Bonino, A. Damin, G. Ricchiardi, M. Ricci, G. Spano, R. D'Aloisio, A. Zecchina, C. Lamberti, C. Prestipino, S. Bordiga, J. Phys. Chem. B, 108 (2004) 3573-3583.

[253] S. Bordiga, F. Bonino, A. Damin, C. Lamberti, Phys. Chem. Chem. Phys., 9 (2007) 4854-4878.

[254] J.A. van Bokhoven, C. Lamberti, Coord. Chem. Rev., 277 (2014) 275-290.

[255] J.C. Doug, H.L. Zhu, Y.J. Xiang, Y. Wang, P.F. An, Y. Gong, Y.X. Lang, L.M. Qiu, A.G. Zheng, X.X. Peng, M. Lin, G.T. Xu, Z.Y. Guo, D.L. Chen, J. Phys. Chem. C, 120 (2016) 20114-20124.

[256] E. Gallo, C. Lamberti, P. Glatzel, Phys. Chem. Chem. Phys., 13 (2011) 19409-19419.

[257] E. Gallo, F. Bonino, J.C. Swarbrick, T. Petrenko, A. Piovano, S. Bordiga, D. Gianolio, E. Groppo, F. Neese, C. Lamberti, P. Glatzel, ChemPhysChem, 14 (2013) 79-83.

[258] C. Li, G. Xiong, Q. Xin, J.K. Liu, P.L. Ying, Z.C. Feng, J. Li, W.B. Yang, Y.Z. Wang, G.R. Wang, X.Y. Liu, M. Lin, X.Q. Wang, E.Z. Min, Angew. Chem.-Int. Edit., 38 (1999) 2220-2222.

[259] C. Li, G. Xiong, J.K. Liu, P.L. Ying, Q. Xin, Z.C. Feng, J. Phys. Chem. B, 105 (2001) 2993-2997.

[260] S. Bordiga, A. Damin, F. Bonino, G. Ricchiardi, C. Lamberti, A. Zecchina, Angew. Chem.-Int. Edit., 41 (2002) 4734-4737.

[261] S. Bordiga, A. Damin, F. Bonino, G. Ricchiardi, A. Zecchina, R. Tagliapietra, C. Lamberti, Phys. Chem. Chem. Phys., 5 (2003) 4390-4393.

[262] Q. Guo, K.J. Sun, Z.C. Feng, G.N. Li, M.L. Guo, F.T. Fan, C. Li, Chem.-Eur. J., 18 (2012) 13854-13860.

[263] Q. Guo, Z.C. Feng, G.N. Li, F.T. Fan, C. Li, J. Phys. Chem. C, 117 (2013) 2844-2848.

[264] C. Lamberti, S. Bordiga, A. Zecchina, A. Carati, A.N. Fitch, G. Artioli, G. Petrini, M. Salvalaggio, G.L. Marra, J. Catal., 183 (1999) 222-231.

[265] G. Artioli, C. Lamberti, G.L. Marra, Acta Crystallogr. Sect. B-Struct. Sci., 56 (2000) 2-10.

[266] C. Lamberti, S. Bordiga, A. Zecchina, G. Artioli, G. Marra, G. Spano, J. Am. Chem. Soc., 123 (2001) 2204-2212.

[267] C.A. Hijar, R.M. Jacubinas, J. Eckert, N.J. Henson, P.J. Hay, K.C. Ott, J. Phys. Chem. B, 104 (2000) 12157-12164.

[268] P.F. Henry, M.T. Weller, C.C. Wilson, J. Phys. Chem. B, 105 (2001) 7452-7458.

[269] M. Signorile, A. Damin, F. Bonin, V. Crocella, G. Ricchiardi, C. Lamberti, S. Bordiga, J. Phys. Chem. C, 122 (2018) 1612-1621.

[270] G.L. Marra, G. Artioli, A.N. Fitch, M. Milanesio, C. Lamberti, Microporous Mesoporous Mat., 40 (2000) 85-94.

[271] R. Dovesi, R. Orlando, A. Erba, C.M. Zicovich-Wilson, B. Civalleri, S. Casassa, L. Maschio, M. Ferrabone, M. De La Pierre, P. D'Arco, Y. Noel, M. Causa, M. Rerat, B. Kirtman, Int. J. Quantum Chem., 114 (2014) 1287-1317.

[272] M. Fischer, Phys. Chem. Chem. Phys., 17 (2015) 25260-25271.

[273] J.P. Wagner, P.R. Schreiner, Angew. Chem.-Int. Edit., 54 (2015) 12274-12296.

[274] M. Fischer, Phys. Chem. Chem. Phys., 18 (2016) 15738-15750.

[275] M. Signorile, A. Damin, F. Bonino, V. Crocella, C. Lamberti, S. Bordiga, J. Comput. Chem., 37 (2016) 2659-2666.

[276] A. Di Cicco, G. Aquilanti, M. Minicucci, E. Principi, N. Novello, A. Cognigni, L. Olivi, J. Phys.: Conf. Ser., 190 (2009) 012043

[277] C. Lamberti, C. Prestipino, S. Bordiga, G. Berlier, G. Spoto, A. Zecchina, A. Laloni, F. La Manna, F. D'Anca, R. Felici, F. D'Acapito, P. Roy, Nucl. Instrum. Methods Phys. Res. Sect. B-Beam Interact. Mater. Atoms, 200 (2003) 196-201.

[278] D. Teschner, J. Borsodi, A. Wootsch, Z. Revay, M. Havecker, A. Knop-Gericke, S.D. Jackson, R. Schlogl, Science, 320 (2008) 86-89.

[279] A.L. Bugaev, A.A. Guda, A. Lazzarini, K.A. Lomachenko, E. Groppo, R. Pellegrini, A. Piovano, H. Emerich, A.V. Soldatov, L.A. Bugaev, V.P. Dmitriev, J.A. van Bokhoven, C. Lamberti, Catal. Today, 283 (2017) 119-126.

[280] A.V. Soldatov, S. Della Longa, A. Bianconi, Solid State Commun., 85 (1993) 863-868.

[281] A.L. Bugaev, V.V. Srabionyan, A.V. Soldatov, L.A. Bugaev, J.A. van Bokhoven, J. Phys.: Conf. Ser., 430 (2013) 012028.

[282] A.L. Bugaev, A.A. Guda, K.A. Lomachenko, V.V. Srabionyan, L.A. Bugaev, A.V. Soldatov, C. Lamberti, V.P. Dmitriev, J.A. van Bokhoven, J. Phys. Chem. C, 118 (2014) 10416-10423.

[283] A.L. Bugaev, A.A. Guda, K.A. Lomachenko, L.A. Bugaev, A.V. Soldatov, Bull. Russ. Acad. Sci: Phys., 79 (2015) 1180-1185.

[284] A.L. Bugaev, A.A. Guda, K.A. Lomachenko, A. Lazzarini, V.V. Srabionyan, J.G. Vitillo, A. Piovano, E. Groppo, L.A. Bugaev, A.V. Soldatov, V.P. Dmitriev, R. Pellegrini, J.A. van Bokhoven, C. Lamberti, J. Phys.: Conf. Ser., 712 (2016) 012032.

[285] A.L. Bugaev, A.A. Guda, K.A. Lomachenko, V.V. Shapovalov, A. Lazzarini, J.G. Vitillo, L.A. Bugaev, E. Groppo, R. Pellegrini, A.V. Soldatov, J.A. van Bokhoven, C. Lamberti, J. Phys. Chem. C, 121 (2017) 18202-18213.

[286] A.L. Bugaev, O.A. Usoltsev, A.A. Guda, K.A. Lomachenko, I.A. Pankin, Y.V. Rusalev, H. Emerich, E. Groppo, R. Pellegrini, A.V. Soldatov, J.A. van Bokhoven, C. Lamberti, J. Phys. Chem. C, 122 (2018) 12029-12037.

[287] A. Bugaev, O.A. Usoltsev, A. Lazzarini, K.A. Lomachenko, A.A. Guda, R. Pellegrini, M. Carosso, J.G. Vitillo, E. Groppo, J.A. van Bokhoven, A.V. Soldatov, C. Lamberti, Faraday Discuss., (2018) doi: 10.1039/C1037FD00211D.

[288] A.L. Bugaev, A.A. Guda, K.A. Lomachenko, E.G. Kamyshova, M.A. Soldatov, G. Kaur, S. Oien-Odegaard, L. Braglia, A. Lazzarini, M. Manzoli, S. Bordiga, U. Olsbye, K.P. Lillerud, A.V. Soldatov, C. Lamberti, Faraday Discuss., (2018) doi: 10.1039/C1037FD00224F.

[289] G. Smolentsev, A. Soldatov, J. Synchrot. Radiat., 13 (2006) 19-29.

[290] G. Smolentsev, A.V. Soldatov, Comput. Mater. Sci., 39 (2007) 569-574.

[291] E. Borfecchia, P. Beato, S. Svelle, U. Olsbye, C. Lamberti, S. Bordiga, Chem. Soc. Rev., 47 (2018) in press.

[292] S.T. Korhonen, D.W. Fickel, R.F. Lobo, B.M. Weckhuysen, A.M. Beale, Chem. Commun., 47 (2011) 800-802.

[293] U. Deka, A.l. Juhin, E.A. Eilertsen, H. Emerich, M.A. Green, S.T. Korhonen, B.M. Weckhuysen, A.M. Beale, J. Phys. Chem. C, 116 (2012) 4809-4818.

[294] U. Deka, I. Lezcano-Gonzalez, B.M. Weckhuysen, A.M. Beale, ACS Catal., 3 (2013) 413-427.

[295] I. Lezcano-Gonzalez, U. Deka, B. Arstad, A. Van Yperen-De Deyne, K. Hemelsoet, M. Waroquier, V. Van Speybroeck, B.M. Weckhuysen, A.M. Beale, Phys. Chem. Chem. Phys., 16 (2014) 1639-1650.

[296] S.A. Bates, A.A. Verma, C. Paolucci, A.A. Parekh, T. Anggara, A. Yezerets, W.F. Schneider, J.T. Miller, W.N. Delgass, F.H. Ribeiro, J. Catal., 312 (2014) 87-97.

[297] E. Borfecchia, K. Lomachenko, F. Giordanino, H. Falsig, P. Beato, A. Soldatov, S. Bordiga, C. Lamberti, Chem. Sci., 6 (2015) 548-563.

[298] T.V. Janssens, H. Falsig, L.F. Lundegaard, P.N. Vennestrøm, S.B. Rasmussen, P.G. Moses, F. Giordanino, E. Borfecchia, K.A. Lomachenko, C. Lamberti, ACS Catal., 5 (2015) 2832-2845.

[299] K.A. Lomachenko, E. Borfecchia, S. Bordiga, A.V. Soldatov, P. Beato, C. Lamberti, J. Phys.: Conf. Ser., 712 (2016) 012041

[300] K.A. Lomachenko, E. Borfecchia, C. Negri, G. Berlier, C. Lamberti, P. Beato, H. Falsig, S. Bordiga, J. Am. Chem. Soc., 138 (2016) 12025-12028.

[301] C. Paolucci, A.A. Parekh, I. Khurana, J.R. Di Iorio, H. Li, J.D. Albarracin Caballero, A.J. Shih, T. Anggara, W.N. Delgass, J.T. Miller, J. Am. Chem. Soc., 138 (2016) 6028-6048.

[302] C. Paolucci, I. Khurana, A.A. Parekh, S. Li, A.J. Shih, H. Li, J.R. Di Iorio, J.D. Albarracin-Caballero, A. Yezerets, J.T. Miller, W.N. Delgass, F.H. Ribeiro, W.F. Schneider, R. Gounder, Science, 357 (2017) 898-903.

[303] M.J. Wulfers, S. Teketel, B. Ipek, R.F. Lobo, Chem. Commun., 51 (2015) 4447-4450.

[304] K. Narsimhan, K. Iyoki, K. Dinh, Y. Román-Leshkov, ACS Cent. Sci., 2 (2016) 424-429.

[305] D.K. Pappas, E. Borfecchia, M. Dyballa, I.A. Pankin, K.A. Lomachenko, A. Martini, M. Signorile, S. Teketel, B. Arstad, G. Berlier, C. Lamberti, S. Bordiga, U. Olsbye, K.P. Lillerud, S. Svelle, P. Beato, J. Am. Chem. Soc., 139 (2017) 14961–14975.

[306] A. Martini, E. Alladio, E. Borfecchia, Top. Catal., (2018) in press.

[307] C. Lamberti, S. Bordiga, M. Salvalaggio, G. Spoto, A. Zecchina, F. Geobaldo, G. Vlaic, M. Bellatreccia, J. Phys. Chem. B, 101 (1997) 344-360.

[308] G.T. Palomino, P. Fisicaro, S. Bordiga, A. Zecchina, E. Giamello, C. Lamberti, J. Phys. Chem. B, 104 (2000) 4064-4073.

[309] F.X. Llabrés i Xamena, P. Fisicaro, G. Berlier, A. Zecchina, G.T. Palomino, C. Prestipino, S. Bordiga, E. Giamello, C. Lamberti, J. Phys. Chem. B, 107 (2003) 7036-7044.

[310] F. Giordanino, P.N.R. Vennestrom, L.F. Lundegaard, F.N. Stappen, S.L. Mossin, P. Beato, S. Bordiga, C. Lamberti, Dalton Trans., 42 (2013) 12741-12761.

[311] P. Glatzel, T.-C. Weng, K. Kvashnina, J. Swarbrick, M. Sikora, E. Gallo, N. Smolentsev, R.A. Mori, J. Electron Spectrosc. Relat. Phenom., 188 (2013) 17-25.

[312] B. Ipek, M.J. Wulfers, H. Kim, F. Göltl, I. Hermans, J.P. Smith, K.S. Booksh, C.M. Brown, R.F. Lobo, ACS Catal., 7 (2017) 4291-4303.

[313] D.K. Pappas, A. Martini, M. Dyballa, K. Kvande, S. Teketel, K.A. Lomachenko, R. Baran, P. Glatzel, B. Arstad, G. Berlier, C. Lamberti, S. Bordiga, U. Olsbye, S. Svelle, P. Beato, E. Borfecchia, J. Am. Chem. Soc., 149 (2018) doi: 10.1021/jacs.1028b08071.

[314] G. Ferey, Chem. Soc. Rev., 37 (2008) 191-214.

[315] J.J. Perry IV, J.A. Perman, M.J. Zaworotko, Chem. Soc. Rev., 38 (2009) 1400-1417.

[316] L. Valenzano, B. Civalleri, S. Chavan, S. Bordiga, M.H. Nilsen, S. Jakobsen, K.P. Lillerud, C. Lamberti, Chem. Mat., 23 (2011) 1700-1718.

[317] M. O'Keeffe, O.M. Yaghi, Chem. Rev., 112 (2012) 675-702.

[318] N. Stock, S. Biswas, Chem. Rev., 112 (2012) 933-969.

[319] T.R. Cook, Y.R. Zheng, P.J. Stang, Chem. Rev., 113 (2013) 734-777.

[320] W.G. Lu, Z.W. Wei, Z.Y. Gu, T.F. Liu, J. Park, J. Park, J. Tian, M.W. Zhang, Q. Zhang, T. Gentle, M. Bosch, H.C. Zhou, Chem. Soc. Rev., 43 (2014) 5561-5593.

[321] V.V. Butova, M.A. Soldatov, A.A. Guda, K.A. Lomachenko, C. Lamberti, Russ. Chem. Rev., 85 (2016) 280-307.

[322] A. Schoedel, M. Li, D. Li, M. O'Keeffe, O.M. Yaghi, Chem. Rev., 116 (2016) 12466-12535.

[323] A. Czaja, T. Trukhan, U. Müller, Chem. Soc. Rev., 38 (2009) 1284-1293.

[324] M. Dinca, J.R. Long, J. Am. Chem. Soc., 127 (2005) 9376-9377.

[325] P.D.C. Dietzel, R.E. Johnsen, H. Fjellvag, S. Bordiga, E. Groppo, S. Chavan, R. Blom, Chem. Commun., (2008) 5125-5127.

[326] J.G. Vitillo, L. Regli, S. Chavan, G. Ricchiardi, G. Spoto, P.D.C. Dietzel, S. Bordiga, A. Zecchina, J. Am. Chem. Soc., 130 (2008) 8386-8396.

[327] L.J. Murray, M. Dinca, J.R. Long, Chem. Soc. Rev., 38 (2009) 1294-1314.

[328] M.P. Suh, H.J. Park, T.K. Prasad, D.W. Lim, Chem. Rev., 112 (2012) 782-835.

[329] M.S. Shah, M. Tsapatsis, J.I. Siepmann, Chem. Rev., 117 (2017) 9755-9803.

[330] X.C. Yang, Q. Xu, Cryst. Growth Des., 17 (2017) 1450-1455.

[331] H. Li, K.C. Wang, Y.J. Sun, C.T. Lollar, J.L. Li, H.C. Zhou, Mater. Today, 21 (2018) 108-121.

[332] J. Lee, O.K. Farha, J. Roberts, K.A. Scheidt, S.T. Nguyen, J.T. Hupp, Chem. Soc. Rev., 38 (2009) 1450-1459.

[333] D. Farrusseng, S. Aguado, C. Pinel, Angew. Chem.-Int. Edit., 48 (2009) 7502-7513.

[334] L.Q. Ma, C. Abney, W.B. Lin, Chem. Soc. Rev., 38 (2009) 1248-1256.

[335] A. Corma, H. Garcıa, F.X. Llabres i Xamena, Chem. Rev., 110 (2010) 4606-4655.

[336] M. Yoon, R. Srirambalaji, K. Kim, Chem. Rev., 112 (2012) 1196-1231.

[337] F.X. Llabrés i Xamena, J. Gascón, Metal Organic Frameworks as Heterogeneous Catalysts, Royal Society of Chemistry, Cambridge, 2013.

[338] D.J. Xiao, E.D. Bloch, J.A. Mason, W.L. Queen, M.R. Hudson, N. Planas, J. Borycz, A.L. Dzubak, P. Verma, K. Lee, F. Bonino, V. Crocella, J. Yano, S. Bordiga, D.G. Truhlar, L. Gagliardi, C.M. Brown, J.R. Long, Nat. Chem., 6 (2014) 590-595.

[339] J.W. Liu, L.F. Chen, H. Cui, J.Y. Zhang, L. Zhang, C.Y. Su, Chem. Soc. Rev., 43 (2014) 6011-6061.

[340] G.W. Zhan, H.C. Zeng, Coord. Chem. Rev., 320 (2016) 181-192.

[341] Y.B. Huang, J. Liang, X.S. Wang, R. Cao, Chem. Soc. Rev., 46 (2017) 126-157.

[342] S.N. Zhao, X.Z. Song, S.Y. Song, H.J. Zhang, Coord. Chem. Rev., 337 (2017) 80-96.

[343] Y.Z. Chen, R. Zhang, L. Jiao, H.L. Jiang, Coord. Chem. Rev., 362 (2018) 1-23.

[344] S. Kempahanumakkagari, K. Vellingiri, A. Deep, E.E. Kwon, N. Bolan, K.H. Kim, Coord. Chem. Rev., 357 (2018) 105-129.

[345] H. Zhang, X.M. Liu, Y. Wu, C. Guan, A.K. Cheetham, J. Wang, Chem. Commun., 54 (2018) 5268-5288.

[346] J.L. Wang, C. Wang, W.B. Lin, ACS Catal., 2 (2012) 2630-2640.

[347] Y.H. Fu, D.R. Sun, Y.J. Chen, R.K. Huang, Z.X. Ding, X.Z. Fu, Z.H. Li, Angew. Chem.-Int. Edit., 51 (2012) 3364-3367.

[348] A. Fateeva, P.A. Chater, C.P. Ireland, A.A. Tahir, Y.Z. Khimyak, P.V. Wiper, J.R. Darwent, M.J. Rosseinsky, Angew. Chem.-Int. Edit., 51 (2012) 7440-7444.

[349] A. Dhakshinamoorthy, A.M. Asiri, H. Garcia, Angew. Chem.-Int. Edit., 55 (2016) 5414-5445.

[350] Y. Chen, V. Lykourinou, T. Hoang, L.J. Ming, S.Q. Ma, Inorg. Chem., 51 (2012) 9156-9158.

[351] Y.H. Shih, S.H. Lo, N.S. Yang, B. Singco, Y.J. Cheng, C.Y. Wu, I.H. Chang, H.Y. Huang, C.H. Lin, ChemPlusChem, 77 (2012) 982-986.

[352] M. Zhao, S. Ou, C.D. Wu, Acc. Chem. Res., 47 (2014) 1199-1207.

[353] J. Huo, J. Aguilera-Sigalat, S. El-Hankari, D. Bradshaw, Chem. Sci., 6 (2015) 1938-1943.

[354] F.K. Shieh, S.C. Wang, C.I. Yen, C.C. Wu, S. Dutta, L.Y. Chou, J.V. Morabito, P. Hu, M.H. Hsu, K.C.W. Wu, C.K. Tsung, J. Am. Chem. Soc., 137 (2015) 4276-4279.

[355] A.H. Chughtai, N. Ahmad, H.A. Younus, A. Laypkov, F. Verpoort, Chem. Soc. Rev., 44 (2015) 6804-6849.

[356] X.Z. Lian, Y. Fang, E. Joseph, Q. Wang, J.L. Li, S. Banerjee, C. Lollar, X. Wang, H.C. Zhou, Chem. Soc. Rev., 46 (2017) 3386-3401.

[357] A. Samui, S.K. Sahu, New J. Chem., 42 (2018) 4192-4200.

[358] P.D.C. Dietzel, Y. Morita, R. Blom, H. Fjellvag, Angew. Chem.-Int. Edit., 44 (2005) 6354-6358.

[359] P.D.C. Dietzel, B. Panella, M. Hirscher, R. Blom, H. Fjellvag, Chem. Commun., (2006) 959-961.

[360] W. Zhou, H. Wu, T. Yildirim, J. Am. Chem. Soc., 130 (2008) 15268-15269.

[361] S.M. Chavan, O. Zavorotynska, C. Lamberti, S. Bordiga, Dalton Trans., 42 (2013) 12586-12595.

[362] M.T. Kapelewski, S.J. Geier, M.R. Hudson, D. Stück, J.A. Mason, J.N. Nelson, D.J. Xiao, Z. Hulvey, E. Gilmour, S.A. FitzGerald, M. Head-Gordon, C.M. Brown, J.R. Long, 136 (2014) 12119-12129.

[363] P.D.C. Dietzel, V. Besikiotis, R. Blom, J. Mater. Chem., 19 (2009) 7362-7370.

[364] Y. Peng, V. Krungleviciute, I. Eryazici, J.T. Hupp, O.K. Farha, T. Yildirim, J. Am. Chem. Soc., 135 (2013) 11887-11894.

[365] S. Chavan, F. Bonino, J.G. Vitillo, E. Groppo, C. Lamberti, P.D.C. Dietzel, A. Zecchina, S. Bordiga, Phys. Chem. Chem. Phys., 11 (2009) 9811-9822.

[366] S.R. Caskey, A.G. Wong-Foy, A.J. Matzger, J. Am. Chem. Soc., 130 (2008) 10870-10871.

[367] W.L. Queen, M.R. Hudson, E.D. Bloch, J.A. Mason, M.I. Gonzalez, J.S. Lee, D. Gygi, J.D. Howe, K. Lee, T.A. Darwish, M. James, V.K. Peterson, S.J. Teat, B. Smit, J.B. Neaton, J.R. Long, C.M. Brown, Chem. Sci., 5 (2014) 4569-4581.

[368] L. Valenzano, B. Civalleri, K. Sillar, J. Sauer, J. Phys. Chem. C, 115 (2011) 21777-21784.

[369] S. Chavan, J.G. Vitillo, E. Groppo, F. Bonino, C. Lamberti, P.D.C. Dietzel, S. Bordiga, J. Phys. Chem. C, 113 (2009) 3292-3299.

[370] E.D. Bloch, M.R. Hudson, J.A. Mason, S. Chavan, V. Crocella, J.D. Howe, K. Lee, A.L. Dzubak, W.L. Queen, J.M. Zadrozny, S.J. Geier, L.C. Lin, L. Gagliardi, B. Smit, J.B. Neaton, S. Bordiga, C.M. Brown, J.R. Long, J. Am. Chem. Soc., 136 (2014) 10752-10761.

[371] F. Bonino, S. Chavan, J.G. Vitillo, E. Groppo, G. Agostini, C. Lamberti, P.D.C. Dietzel, C. Prestipino, S. Bordiga, Chem. Mat., 20 (2008) 4957-4968.

[372] L. Valenzano, J.G. Vitillo, S. Chavan, B. Civalleri, F. Bonino, S. Bordiga, C. Lamberti, Catal. Today, 182 (2012) 67-79.

[373] E.D. Bloch, L.J. Murray, W.L. Queen, S. Chavan, S.N. Maximoff, J.P. Bigi, R. Krishna, V.K. Peterson, F. Grandjean, G.J. Long, B. Smit, S. Bordiga, C.M. Brown, J.R. Long, J. Am. Chem. Soc., 133 (2011) 14814-14822.

[374] S. Chavan, F. Bonino, L. Valenzano, B. Civalleri, C. Lamberti, N. Acerbi, J.H. Cavka, M. Leistner, S. Bordiga, J. Phys. Chem. C, 117 (2013) 15615-15622.

[375] B. Van de Voorde, M. Hezinová, J. Lannoeye, A. Vandekerkhove, B. Marszalek, B. Gil, I. Beurroies, P. Nachtigall, D. De Vos, Phys. Chem. Chem. Phys., 17 (2015) 10759-10766.

[376] G. Kresse, J. Furthmuller, Phys. Rev. B, 54 (1996) 11169-11186.

[377] G. Kresse, D. Joubert, Phys. Rev. B, 59 (1999) 1758-1775.

[378] J. Hafner, J. Comput. Chem., 29 (2008) 2044-2078.

[379] J.P. Perdew, K. Burke, M. Ernzerhof, Phys. Rev. Lett., 77 (1996) 3865-3868.

[380] K. Hayakawa, K. Hatada, P. D'Angelo, S. Della Longa, C.R. Natoli, M. Benfatto, J. Am. Chem. Soc., 126 (2004) 15618-15623.

[381] A. Bianconi, M. Dell'Ariccia, A. Gargano, C.R. Natoli, Bond Length Determination Using XANES, in: A. Bianconi, L. Incoccia, S. Stipcich (Eds.) EXAFS and Near Edge Structure. Springer Series Chem. Phys., vol 27. , Springer, Berlin, 1983, pp. 57-61.

[382] C.R. Natoli, Distance Dependence of Continuum and Bound State of Excitonic Resonances in X-Ray Absorption Near Edge Structure (XANES), in: K.O. Hodgson, B. Hedman, J.E. Penner-Hahn (Eds.) EXAFS and Near Edge Structure III. Springer Proc. Phys., Vol 2. , Springer, Berlin, 1984, pp. 38-42.

[383] J.G. Chen, Surf. Sci. Rep., 30 (1997) 1-152.

[384] G. Hahner, Chem. Soc. Rev., 35 (2006) 1244-1255.

[385] H. Ade, H. Stoll, Nat. Mater., 8 (2009) 281-290.

[386] M. Havecker, M. Cavalleri, R. Herbert, R. Follath, A. Knop-Gericke, C. Hess, K. Hermann, R. Schlogl, Phys. Status Solidi B-Basic Solid State Phys., 246 (2009) 1459-1469.

[387] R. Toyoshima, H. Kondoh, J. Phys.-Condes. Matter, 27 (2015) 083003.

[388] G.A. Somorjai, S.K. Beaumont, S. Alayoglu, Angew. Chem.-Int. Edit., 50 (2011) 10116-10129.

[389] C. Castan-Guerrero, D. Krizmancic, V. Bonanni, R. Edla, A. Deluisa, F. Salvador, G. Rossi, G. Panaccione, P. Torelli, Rev. Sci. Instrum., 89 (2018) 054101.

[390] F. Borgatti, P. Torelli, M. Brucale, D. Gentili, G. Panaccione, C.C. Guerrero, B. Schafer, M. Ruben, M. Cavallini, Langmuir, 34 (2018) 3604-3609.

[391] P. Glatzel, R. Alonso-Mori, D. Sokaras, Hard X-Ray Photon-in/Photon-out Spectroscopy: Instrumentation, Theory and Applications, in: J.A. van Bokhoven, C. Lamberti (Eds.) X-Ray Absorption and X-Ray Emission Spectroscopy: Theory and Applications, John Wiley & Sons, Chichester (UK), 2016, pp. 125-153.